

# A Search for Neutral Long-Lived Particles

Todd Adams  
Florida State University

DØ Note XXXX  
Version 1.5

November 21, 2005

## Abstract

We present a search for a neutral particle pair produced in  $p\bar{p}$  collisions at  $\sqrt{s}=1.96$  TeV which decays to two muons and a neutrino and lives long enough to travel at least 5 cm before decaying. The analysis uses  $383 \text{ pb}^{-1}$  of data and represents a preliminary result for conference presentation.

## 1 Introduction

The large data samples available at DØ from Run II facilitate new searches which were previously unexplored. Here, we present a search for a neutral particle which travels at least 5 cm before decaying to two muons and a neutrino. The particle is assumed to have a mass as low as several GeV and a decay length greater than several cm. The production cross-section must be fairly small for such a particle to have escaped detection during Run I, LEP I & II and numerous fixed target experiments. In addition, the state can not contribute to the invisible width of the  $Z$ .

This analysis is motivated by an experimental result from NuTeV [1], by an unexplored region of supersymmetry (SUSY) parameter space, and by our desire to expand the discovery potential of DØ. The goal is to search for the pair production of two neutral, long-lived particles (NLLP) (Fig. 1) which decay to two charged leptons and a neutrino (Fig. 2).

In this note we will first give the motivation and describe the strategy for this analysis including a previous study demonstrating our ability to find highly displaced vertices. Then we will discuss studies with signal and background Monte Carlo. This is followed by documentation on the data set and the selection criteria. The last sections will detail the background estimate and cross-section limit sensitivity. At this point the analysis is still a “closed box” in that the signal region has not been searched.



Figure 1: Feynman diagrams for pair production of a neutral particle, in this case a pair of neutralinos. It is expected that the left diagram will not contribute due to limits on the invisible width of the  $Z$ .

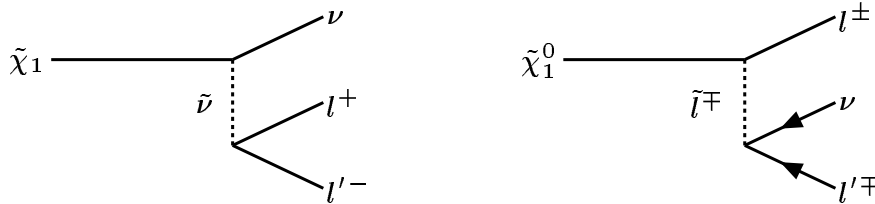


Figure 2: Feynman diagrams for decay of a neutral particle to two muons and a neutrino, in this case a neutralino decay.

## 1.1 NuTeV Result

NuTeV performed several searches using a low mass decay region in front of the neutrino target/detector. Neutral particles coincident with the neutrino beam can enter this region and decay. Interspersed drift chambers allow for tracking and vertexing. The neutrino detector is used for particle identification and energy measurement. Three searches were performed covering masses of 0.033 GeV [2], 0.25-2.0 GeV [3], and 2.2-15 GeV [1]. The first two searches were consistent with no signal and limits were set on the Karmen anomaly [4] and on neutral heavy lepton (NHL) production. The third search found 3 dimuon events with an expected standard model background of  $0.07 \pm 0.01$  events.

There is no widely-accepted, published explanation of this excess. If interpreted as new physics, several interesting things should be noted. The particle is likely to have been produced in collisions of the 800 GeV proton beam with the fixed BeO target located 1.4 km upstream of the detector. There exists  $>1$  km of dirt and shielding between this production point and the detector. Therefore, the particle must be long lived and interact rarely. The observation is consistent with a particle of mass 5 GeV, although this could be as large as  $\sim 15$  GeV, limited by the proton-proton  $\sqrt{s}=38$  GeV. The dimuon events have missing transverse energy consistent with an unobserved neutrino. However, the events are also very asymmetric in the energies of the two muons which is unexpected in a decay. In the end, NuTeV chose to set a limit (see Fig. 3).

$D\bar{O}$  has the ability to look for such particles, although a specific production model is required to compare results directly with those of NuTeV.  $D\bar{O}$  has a significantly increased center-of-mass ( $\sqrt{s} = 38 \rightarrow 1960$  GeV) and (assuming pair production through annihilation) benefits from the valence anti-quarks. The  $D\bar{O}$  search complements the NuTeV analysis by being sensitive to shorter lifetimes (see Sec. 8.1).

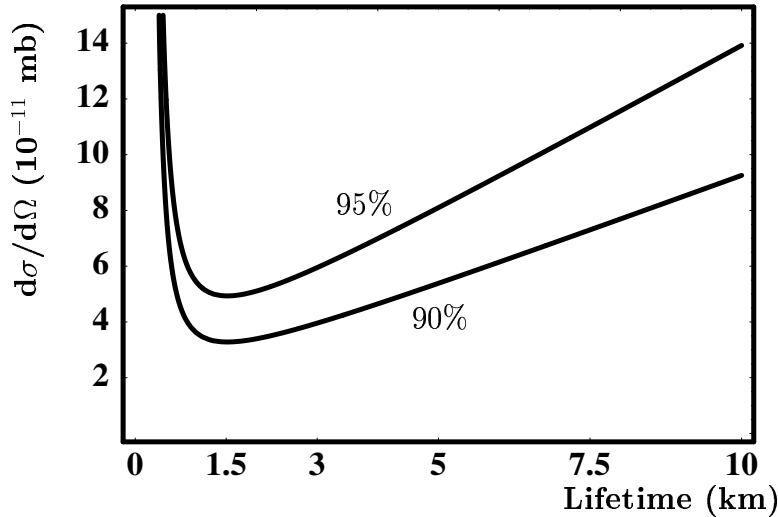


Figure 3: Limit of neutral particle pair production at the primary target at NuTeV. This figure is taken from [1].

## 1.2 Theoretical Possibilities

Many models of supersymmetry are favored by theoreticians and experimentalists for reasons such as having fewer parameters (mSUGRA) or providing a dark matter candidate (R-parity conservation). However these ideas are not established laws and supersymmetry can exist in other forms. It has been shown that there is a portion of supersymmetric parameter space that is not excluded by previous experiments [5]. Collider experiments such as those at LEP and the Tevatron are designed to detect stable particles that originate from near the center of the detector. A neutral, weakly interacting, long-lived particle will go largely undetected. Previously it would only be evidenced in searches as missing transverse energy or as decays very close to the primary interaction region [6]. In this analysis we look for direct evidence via highly displaced vertices.

For this search, we are interested in a model of unconstrained MSSM (uMSSM) with R-parity violation. By unconstrained we mean relaxing the requirement of GUT-scale unification. In these models, the neutralino is the lightest supersymmetric particle (LSP) and is allowed to decay to two charged leptons ( $e$  and/or  $\mu$ ) and a neutrino. However, if certain couplings are small the neutralino lifetime can become significant. An example model is presented in Sec. 3.

## 2 Analysis Strategy

We will use the volume inside the DØ central fiber tracker as a decay region. This allows the full CFT and muon systems to be used for detecting the decay products. By including all layers of the CFT we avoid the need to modify the tracking algorithms which dramatically reduces the necessary work.

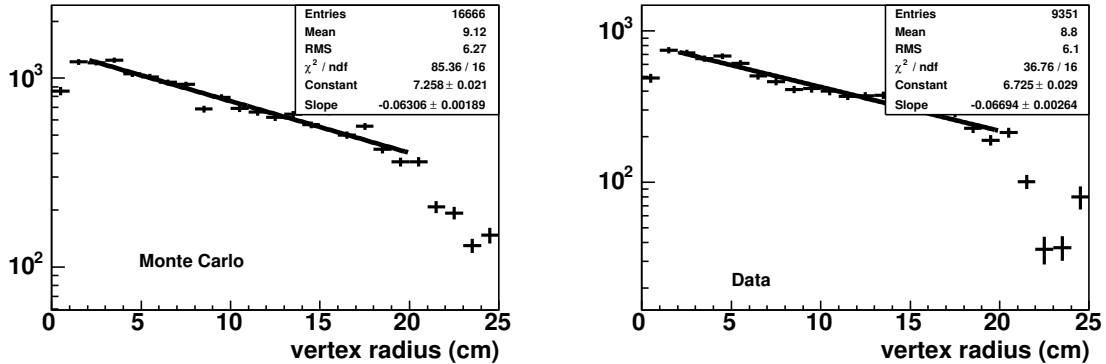


Figure 4: Distribution of the radius of reconstructed vertex of  $K_s$  candidates. The left plot is Monte Carlo, the right plot is data. Here same sign combinatoric background has been subtracted from opposite sign events. The distributions are fit to an exponential.

The strategy is to identify events with a pair of good, isolated muons with centrally matched tracks. Each pair is fit to a vertex using DØRoot. The final sample consists of events with good muon vertices that are displaced 5-20 cm (in the transverse plane) from the primary vertex. We define the variable

$$r = \sqrt{(v_x - v_x(PV))^2 + (v_y - v_y(PV))^2} \quad (1)$$

where  $v_x, v_y$  are the  $x, y$  positions of the fitted muon vertex and  $v_x(PV), v_y(PV)$  are the  $x, y$  positions of the primary vertex (PV).

## 2.1 $K_s$ Studies

A study was performed to demonstrate DØ's ability to reconstruct vertices at large radial displacement. The primary source of such vertices are  $K_s \rightarrow \pi^+ \pi^-$  decays. QCD data and MC events were used to show that DØ code finds vertices out to  $>20$  cm (Fig. 4). The following conclusions are drawn:

1. the MC efficiency is close to flat in the range  $r = 5-20$  cm (Fig. 5)
2. the ratio of data to MC efficiency is flat over this region (Fig. 6)
3. the slopes are consistent with the  $K_s$  lifetime appropriately boosted (Fig. 4).

This allows us to proceed with the planned analysis with confidence in DØ's ability to find a signal with vertices far from the production vertex. The full study is available in DØ Note 4761 [7], however the plots included here have been re-generated with a slightly different Monte Carlo sample including small improvements in statistics.

The ratio of Monte Carlo to data in Fig. 6 is 1.75 which is a function of both the reconstruction efficiency and the number of  $K_s$ 's in each sample. A study was done to separate the vertex reconstruction efficiency from the number of  $K_s$ 's. We use the same QCD samples and calculate the invariant mass of all pairs of central tracks without using any vertex information. Figure 7 shows the resulting distributions with a fit to

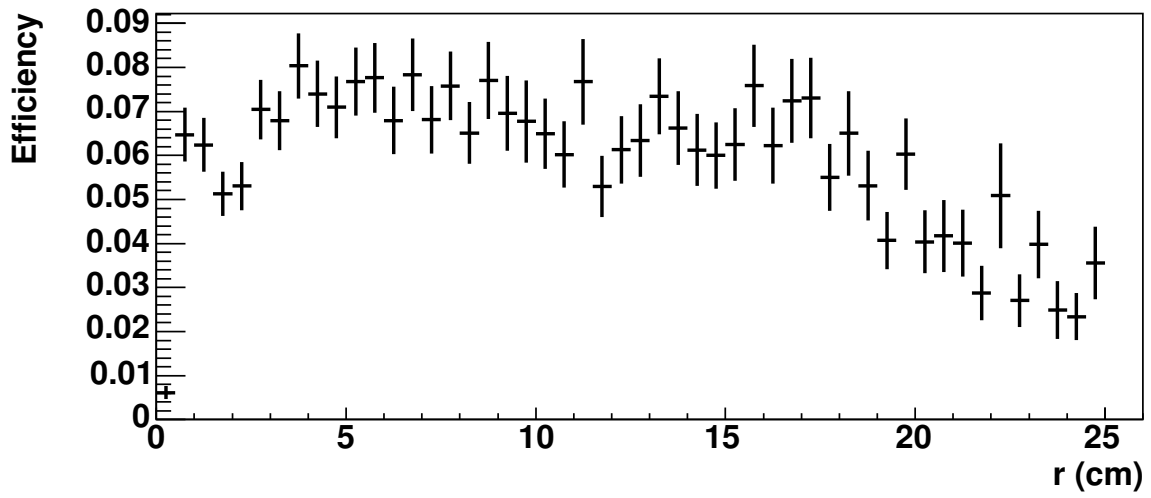


Figure 5:  $K_s$  reconstruction efficiency as a function of generated vertex radius.

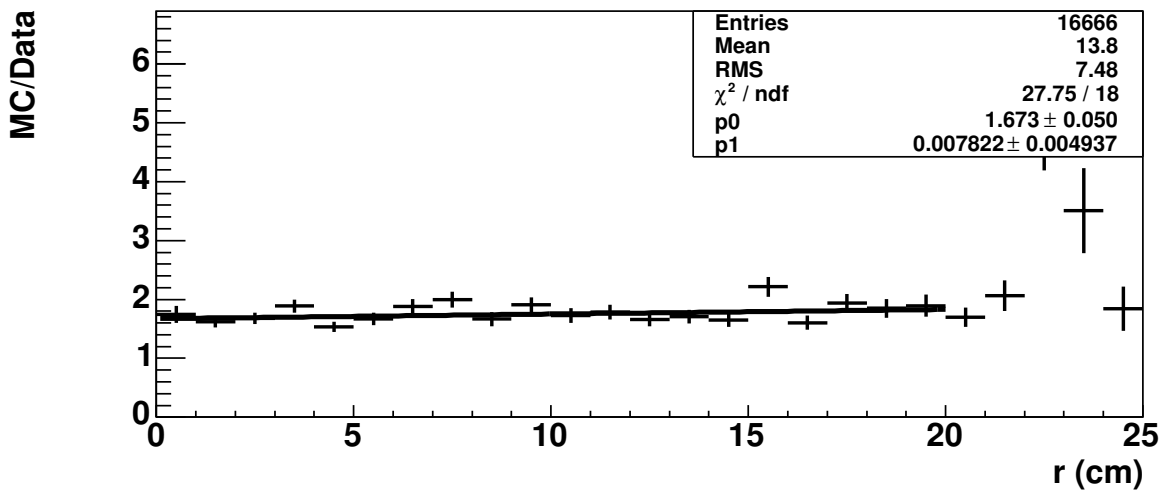


Figure 6: Ratio of number of reconstructed vertices for Monte Carlo to data as a function of vertex radius for  $K_s$  candidates.

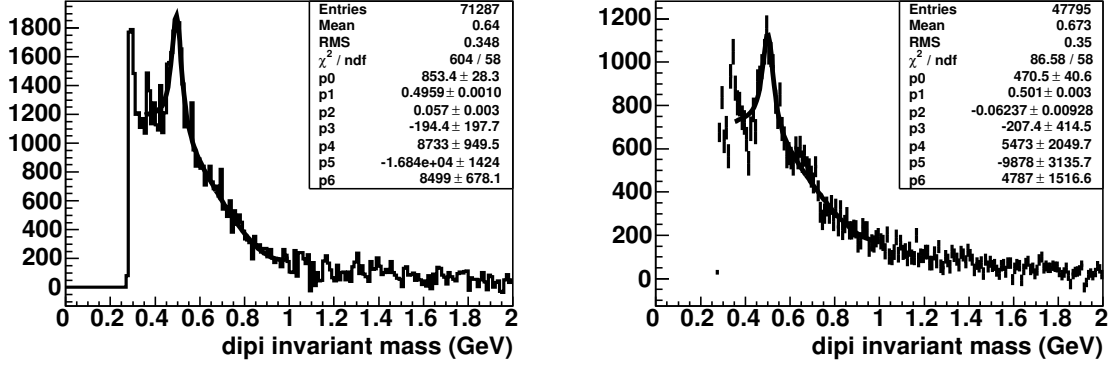


Figure 7: Distribution of the invariant mass of all central tracks for the QCD Monte Carlo (left) and QCD data (right). The same-signed events have been subtracted from the opposite-signed events. The mass range 0.35-1.0 is fit to a Breit-Wigner plus a 4th order polynomial.

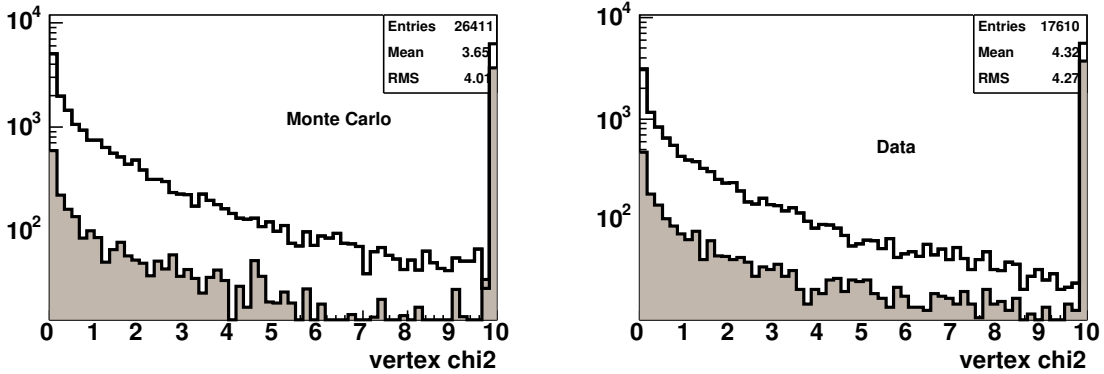


Figure 8: Distribution of the vertex  $\chi^2$  for  $K_s$  candidates for Monte Carlo (left) and data (right). The open histogram is opposite-signed pairs while the filled histogram is for same-signed pairs. The rightmost bin includes overflows.

a Breit-Wigner (B-W) plus a 4th order polynomial. Numerical integration of the B-W yields  $6852 \pm 25$  events for Monte Carlo and  $4136 \pm 50$  events for data. This results in a ratio (MC/data) of  $K_s$  candidates (without vertexing) of  $1.66 \pm 0.21$  which is consistent with the ratio in Fig. 6. We will later use these numbers to determine a data/MC correction factor for vertex reconstruction.

Additional comparisons between  $K_s$  candidates for MC and data are provided in Figs. 8-10. This analysis will use the vertex  $\chi^2$  and the track distance of closest approach (Sec. 6.2.2). Figures 11 and 12 show the ratio of MC to data for these variables which are generally flat. The track DCA ratio differs from the nominal 1.75 of the radius and vertex  $\chi^2$  distribution because it is also dependent upon the number of vertices.

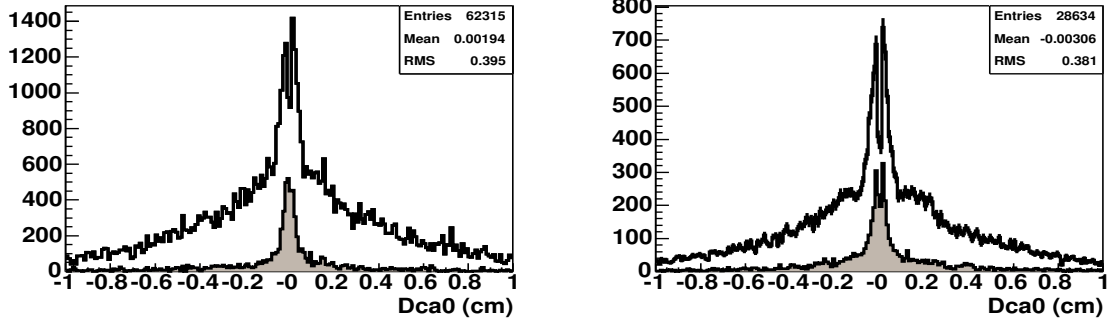


Figure 9: Distribution of the DCA0 (x-y plane) for  $K_s$  candidates for Monte Carlo (left) and data (right). The open histogram is opposite-signed pairs while the filled histogram is for same-signed pairs.

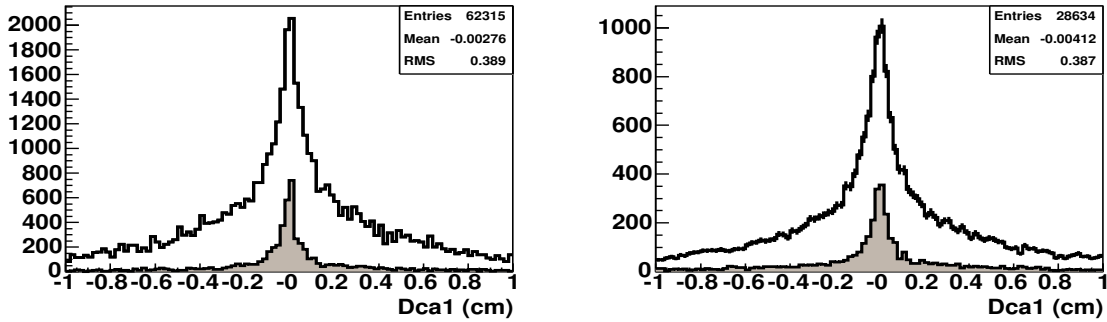


Figure 10: Distribution of the DCA1 (z axis) for  $K_s$  candidates for Monte Carlo (left) and data (right). The open histogram is opposite-signed pairs while the filled histogram is for same-signed pairs.

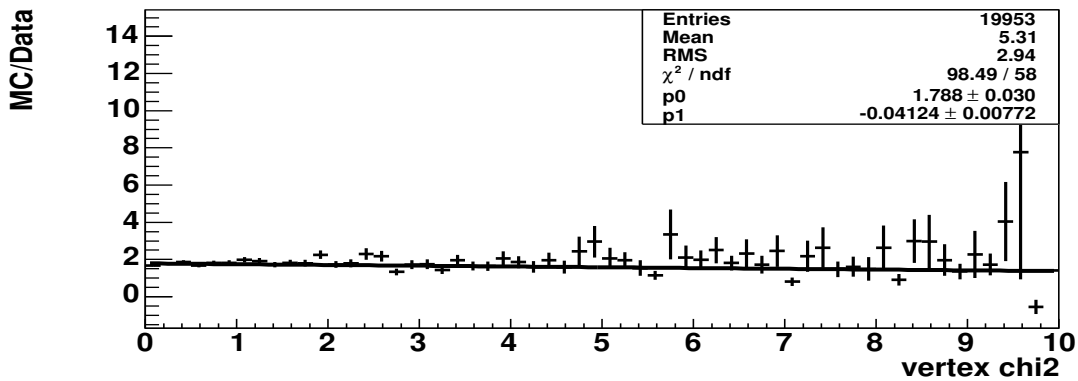


Figure 11: Ratio of MC/data for the vertex  $\chi^2$  for  $K_s$  candidates.

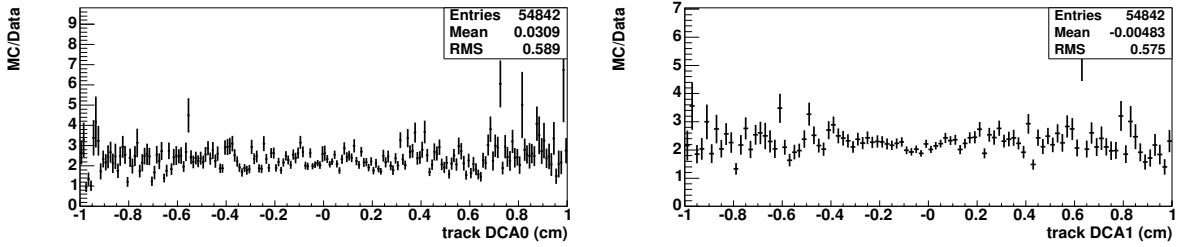


Figure 12: Ratio of MC/data for the DCA0 (right) and DCA1 (left) for  $K_s$  candidates.

### 3 Signal Monte Carlo

Signal Monte Carlo events have been generated using a SUSY point that allows pair production of low mass neutralinos with a long lifetime and subsequent decays to  $\mu^+\mu^-\nu$ . The unconstrained minimal supersymmetric model with R-parity violation (RPV) [8] is used with the parameters listed in Table 1.

The neutralino mass is determined primarily from  $M_1$  and  $R_S$  (the gauge mass unification breaking scale). The lifetime is related to the parameter  $\lambda_{122}$ . We account for the decay rate in the final result by interpreting it as a function of cross-section  $\times$  branching ratio and lifetime. Therefore, during generation we require that one neutralino decay within the cylindrical volume given by  $r < 25$  cm ( $r$  is the radial distance from the beamline). This region will be the focus of the analysis (Sec. 2). The other neutralino is forced to decay well outside the detector. Neutralinos are allowed to decay to  $\mu^+\mu^-\nu$ ,  $e^+e^-\nu$  or  $e^\pm\mu^\mp\nu$ .

Multiple sets were created using the SUSYGEN program [9] with different masses in the range 3-10 GeV. All samples are run through the standard simulation chain using p14.07.00/p14.06.01 with a minimum bias contribution of 0.4 events per beam crossing. Monte Carlo smearing is discussed in Sec. 4.3.1. Unless noted, signal Monte Carlo refers to Set 2 (mass = 5 GeV).

Figures 13 and 14 show some generated and reconstructed variables of interest for the signal samples. The average  $p_T$  of all the samples is approximately 85 GeV, while the opening angle is seen to increase with  $\chi_1^0$  mass.

Figure 15 shows the invariant mass from the various signal samples. This reconstructed mass (left plot) is made using the smeared muon four vectors as measured at the primary vertex. The presence of the unobserved neutrino causes the dimuon mass to be reconstructed lower (on average) than the neutralino mass while the muon resolution and incorrect vertex creates a broadening of the reconstructed mass.

## 4 Standard Model Sources and Studies

### 4.1 Physics Processes

There are a number of sources of dimuon events in this low mass region. Standard Model sources include

Table 1: SUSY parameters used for Monte Carlo generation.

Parameter	Set 1	Set 2	Set 3	Set 4
Inputs				
$\tan\beta$	10	10	10	10
$\mu$	-5000	-5000	-5000	-5000
$R_S$	1.0	1.0	1.0	1.0
$M_1$ (GeV)	3	5	8	10
$M_2$ (GeV)	200	200	200	200
$M_3$ (GeV)	400	400	400	400
$M_{squark}$ (GeV)	300	300	300	300
$M_{sbottom,stop}$ (GeV)	1500	1500	1500	1500
$\lambda_{122}$	0.01	0.01	0.01	0.01
Outputs				
$M_{\chi_0^1}$ (GeV)	3.07	5.08	8.08	10.08
Lifetime $\chi_0^1$ (cm)	305576	24787	2425	802
Cross-section (pb)	0.025	0.024	0.023	0.022
Number of generated events	32000	31000	32000	33000

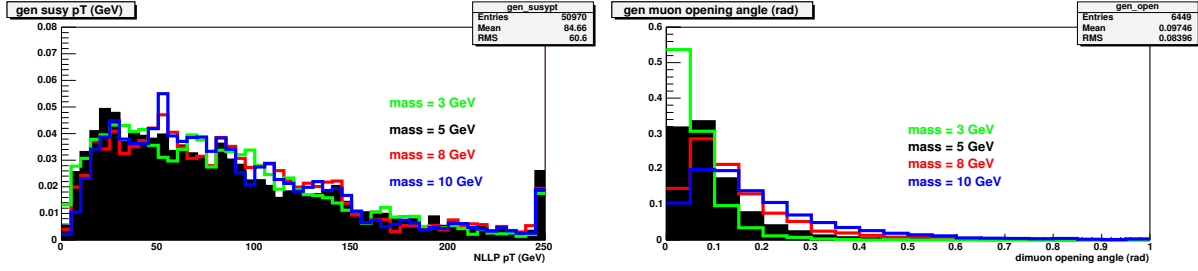


Figure 13: Distributions of generated  $\chi_1^0$   $p_T$  (left) and opening angle between the muons (right) for various SUSY parameter sets. All histograms are normalized to an area of 1. The rightmost bin includes all overflows.

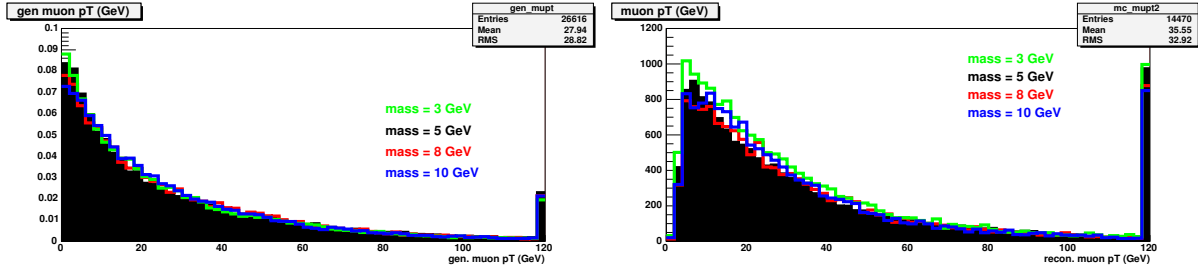


Figure 14: Distributions of generated muon  $p_T$  (left) and reconstructed muon  $p_T$  for various SUSY parameter sets. The statistics box represents information for Set 2. All histograms are normalized to an area of 1. The rightmost bin includes all overflows.

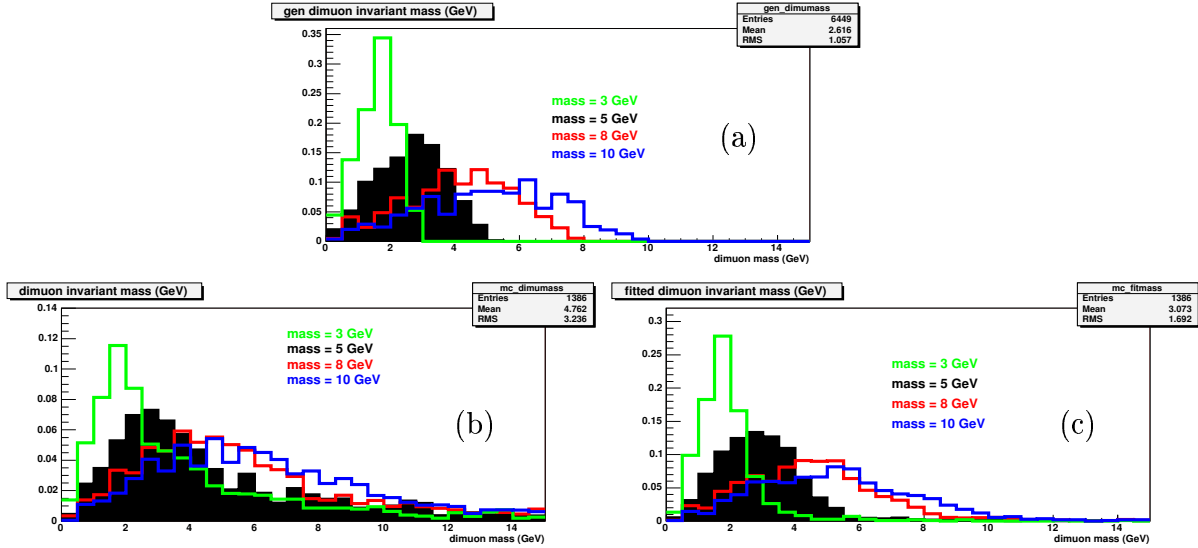


Figure 15: Distributions of invariant dimuon mass for different SUSY parameter sets. All histograms are normalized to an area of 1. The top plot (a) shows the generated dimuon mass. The left plot (b) shows the mass reconstructed with the smeared muon  $p_T$ . The right plot (c) represents the mass after vertex fitting.

1.  $J/\psi \rightarrow \mu^+ \mu^-$
2.  $\psi(2S) \rightarrow \mu^+ \mu^-$
3.  $\Upsilon(1S) \rightarrow \mu^+ \mu^-$
4.  $\Upsilon(2S) \rightarrow \mu^+ \mu^-$
5.  $\Upsilon(3S) \rightarrow \mu^+ \mu^-$
6.  $Drell - Yan \rightarrow \mu^+ \mu^-$
7.  $b\bar{b} \rightarrow \mu^+ \nu \mu^- \nu c\bar{c}$
8.  $b\bar{b} \rightarrow \mu^- \nu c\bar{b} \rightarrow \mu^- \nu \mu^+ \nu s\bar{b}$  (and charge conjugate)
9.  $K_s \rightarrow \pi^+ \pi^- \rightarrow \mu^+ \nu \mu^- \nu$

where any of these can be associated with additional jet activity. It is also possible to produce  $J/\psi$ ,  $\psi(2S)$  and  $\Upsilon(1S, 2S, 3S)$  from decays in  $b\bar{b}$  production.

We will use our selection criteria to reduce these backgrounds significantly (see Sec. 7) including muon  $p_T > 10$  GeV, dimuon opening angle  $< 0.5$  radians and a cut on the minimum distance of closest approach (DCA). Muon  $p_T$  and opening angle cuts select only events with a significant Lorentz boost (for processes such as (1)-(6) and (9)). Process (7) is removed by the opening angle cut while process (8) is restricted by the muon  $p_T$  cut. The DCA cut further eliminates muons coming from any reconstructed vertex near the beamline.

There are also several sources of long-lived, unstable particles which may result in detached vertices:

1.  $K_s \rightarrow \pi^+ \pi^- \rightarrow \mu^+ \nu \mu^- \nu$

2.  $\Lambda_c^\pm \rightarrow \Lambda \mu \nu \rightarrow \mu \nu p \mu \nu$
3.  $\Lambda^0 \rightarrow p \mu \nu$
4.  $\Sigma^\pm \rightarrow n \mu \nu$
5.  $\Xi^0 \rightarrow p \mu \nu$
6.  $\Xi^\pm \rightarrow n \mu \nu$

All of the hadrons (except the  $\Lambda_c$ ) have branching fractions to muons in the  $10^{-4} - 10^{-5}$  range. Of these, only the first two can result in a real two muon state and even then the muons do not originate from the same vertex.

A generator level study of  $\Lambda \rightarrow p \mu \nu$  was carried out. Using Pythia [10] we replace the  $\Lambda \rightarrow p e \nu$  decay mode with the semi-muonic one and turn off all other decays. Fifty million QCD events were generated which approximates the luminosity of this analysis when the  $2 \times 10^{-4}$  branching fraction is accounted for. Only 28 events had a  $\Lambda$  decay with a generator level  $p_T > 5$  GeV muon within a cylindrical volume of  $r < 50$  cm and  $\ell < 4$  m. Therefore we estimate the contribution to this analysis is negligible when we require 2 reconstructed muons with  $p_T > 10$  GeV vertexing within 20 cm of the beamline.

## 4.2 Mis-reconstruction

Fake dimuon events arise when a single real muon is present and another track is matched to a fake candidate in the muon system. We will see in Fig. 30 that the ratio of same-signed to opposite-signed candidates show that random combinatorics is not an issue.

Several steps are taken to reduce the fake contribution. The central tracks appear real as they generally have 16 CFT hits and a good  $\chi^2$ . A cut requiring the local muon candidates be at least 1 cm apart removes muon pairs having two central tracks matched to the same A and BC wire hits. The opening angle distribution does not have a peak at opening angle = 0 (see Fig. 29) which shows we do not have the case of one central track matched to two different sets of muon hits. Requiring both tracks to have a minimum distance of closest approach (DCA) dramatically decreases both the SM and fake backgrounds since they likely originate from the primary vertex.

## 4.3 Z/DY Studies

The Z/DY background is used to verify the data set is complete and determine the nature of data/MC corrections. Previous versions of this analysis had shown differences between data and MC. Several studies were carried out to resolve/quantify these differences.

It was discovered that a portion of the data ( $< 10\%$ ) was missing from the results presented prior to July 2005. This was exasperated by the loss of some of the original subskim records. The data was been subsequently re-subskimmed (Sec. 5 has been updated) with the input number of events verified to match the output of the previous stage. Complete records are now available.

Table 2: Parameters for trigger acceptance.

	A0	A1	A2	A3
L1 mulptxatxx	$-0.8 \pm 0.2$	$2.8 \pm 0.5$	$0.1 \pm 0.1$	$0.99 \pm 0.01$

The Z/DY events are reweighted by dimuon  $p_T$  as described by the analysis of Tiller and Nunnemann [11]. As recommended, the values determined for the 60-130 GeV mass range are applied to all mass bins in this analysis. The distributions are also renormalized such that they give the same area as before reweighting.

The trigger acceptance has been estimated from the Top Trigger analysis [12]. The efficiency of the L1 trigger term on which all dimuon triggers are based (mu2ptxatxx) comes from the multiplication of the parameterized efficiency for mulptxatxx applied to each muon:

$$Eff(\eta) = A3 + A0 \times \exp(-A1 \times (\eta^2 - A2^2)) \times \sin(\eta^2 - A2^2) \quad (2)$$

where the values for the parameters A0-A3 are found in DØ Note 4512 [12] and listed in Table 2. The L2 efficiency is taken to be flat in  $p_T$  and  $\eta$  with a value of  $0.98 \pm 0.007$ . The L3 efficiency has been measured (by the Top group) to be 100% for trigger list v8-v12. We assign a systematic error of 3% since the trigger analysis has not been repeated for this analysis.

#### 4.3.1 Muon $p_T$ Smearing

This analysis requires modified smearing for the muon  $p_T$ . For tracks with no SMT hits, the standard MC is smeared to match the  $p_{Tcorr}$  variable in data. However, this variable assumes the primary vertex as a point on the track. The detached nature of the signal decays makes this undesirable. Therefore, we have found a modified smearing to use the  $p_T$  variable for all tracks.

With the help of Raimund Stoeher, new smearing parameters were determined using Z/DY data with  $p_T > 10$  GeV. We use the function:

$$\frac{1}{p_{Tnew}} = \frac{1.008}{p_T} + \left(A + \frac{B}{p_T}\right) \times Gaussian \quad (3)$$

where *Gaussian* refers to a random number thrown with a Gaussian distribution (width = 1). The smearing parameters are listed in Table 3.

The results of this smearing are shown in Fig. 16. The distributions show the significant difference in the resolution with and without SMT hits. The MC has a higher efficiency for finding SMT hits. Therefore, to match the complete datasets, we renormalize the MC so that the ratio of tracks with  $N_{smt}=0/N_{smt}>0$  matches data. This has been done for the upper plots and lower right plot in Fig. 16, while the lower left plot does not modify the MC ratio. However, this adjustment is not applied in the rest of the analysis due to a bias in the MC  $z$  vertex distribution for tracks without SMT hits.

Table 3: Parameters used for muon  $p_T$  smearing.

	A	B
$N_{smt \neq 0}  \eta  < 1.5$	0.0016	0.0192
$N_{smt \neq 0}  \eta  > 1.5$	0.0019	0.0231
$N_{smt=0}$	0.004	0.08

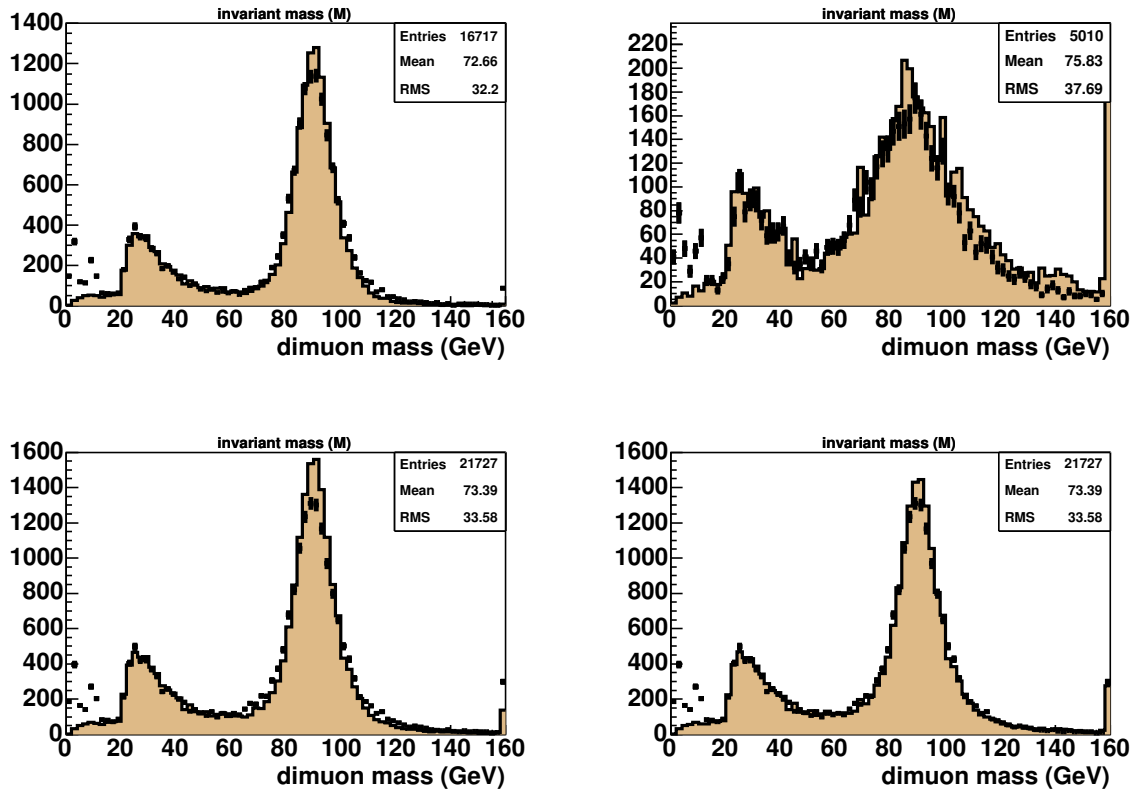


Figure 16: Distribution of dimuon invariant mass with cuts listed in 4.3.2. The points show data while the shaded histogram shows the Z/DY MC for the 2-15, 15-60 and 60-130 GeV mass bins. The upper plots show the distributions for  $N_{smt} > 0$  (left) and  $N_{smt} = 0$  (right). The lower left plot shows all events data while the lower right plot has the ratio of  $(N_{smt} = 0)/(N_{smt} > 0)$  in MC adjusted to match the data.

Table 4: Luminosity associated with different versions of *d0reco*.

<i>d0reco</i> Version	Luminosity
p14.03.00	8.6 pb <sup>-1</sup>
p14.03.01	23.6 pb <sup>-1</sup>
p14.03.02	38.5 pb <sup>-1</sup>
p14.05.00	44.5 pb <sup>-1</sup>
p14.05.02	49.5 pb <sup>-1</sup>
p14.06.00	177.3 pb <sup>-1</sup>
p14.06.01	48.5 pb <sup>-1</sup>

### 4.3.2 RECO Version Comparisons

The data has been reconstructed with 7 different versions of *d0reco* (Table 4). Each of these data sets are somewhat biased with respect to each other since contiguous blocks of run numbers would be processed with the same reco version. An example is the complete p14.06.01 data was taken with the v13 trigger list.

A test was performed to select  $Z \rightarrow \mu\mu$  events with basic cuts:

- no bad runs, good calorimeter quality, dimuon trigger, good primary vertex
- 2 “loose” muons with  $p_T > 10$  GeV,  $n_{\text{seg}} = 3$ , cosmic ray timing cut, calorimeter and track  $p_T$  isolation  $< 2.5$  GeV, central track match with track  $\chi^2 < 4$  and  $N_{\text{CFT}} > 13$

Each of the different reco data sets was run independently and normalized with the inverse of its luminosity so that all samples should have the same area. Figure 17 shows the dimuon mass distribution for each of these sets. Originally it was seen that two of the data sets (p14.03.01 and p14.03.02) were smaller than the rest. This was traced to a mistake in using one of the triggers over the wrong run range. After fixing this (Fig. 17), all areas are seen to be equivalent. This shows (within the limit of agreement in Fig. 17) that there are no missing blocks of data. Also, from the time dependence of the reco versions, we observe no strong run number or trigger version dependence.

### 4.3.3 Data/MC Corrections

We use the Z peak to measure data/MC corrections. Again we use a loose set of criteria:

- no bad runs, dimuon trigger
- 2 “loose” muons with  $p_T > 10$  GeV,  $n_{\text{seg}} = 3$ , calorimeter isolation  $< 4$  GeV, central track match with  $N_{\text{cft}} > 7$ , reject cosmic ray muons with a timing cut.

where data/MC corrections should be minimal. We normalize the Z/DY MC (M=60-130 GeV sample) to the data using the cross-section (185 pb), the K-factor (1.39), the luminosity (48.5 or 383 pb<sup>-1</sup>) and the number of generated events (87,500). Figure 18 shows the result using the p14.06.01 data sample (48.5 pb<sup>-1</sup>). The MC is found to be 1% smaller in the 60-120 GeV range, well within the 6.5% luminosity error.

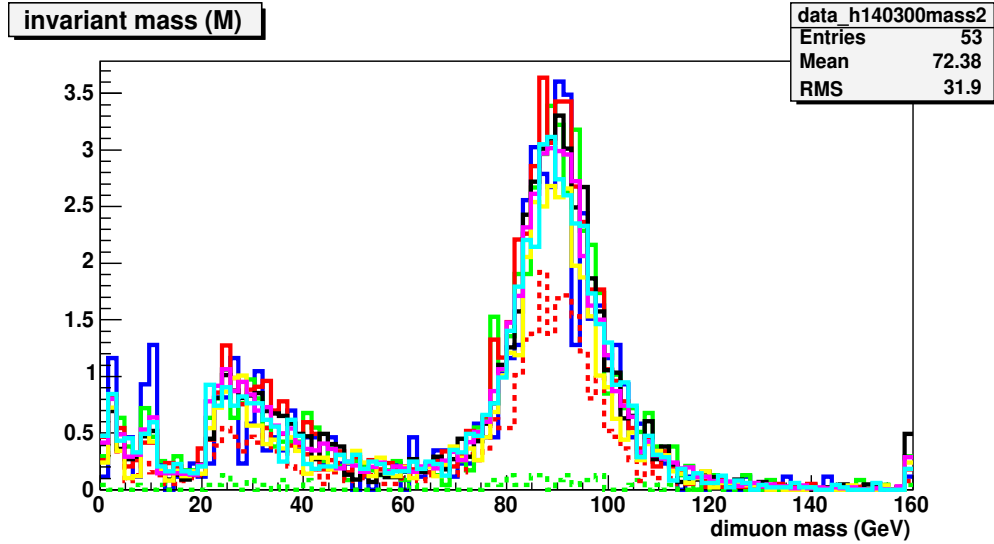


Figure 17: Distribution of the dimuon invariant mass for various versions of *d0reco*: p14.03.00 (blue), p14.03.01 (green), p14.03.02 (red), p14.05.00 (black), p14.05.02 (yellow), p14.06.00 (purple), p14.06.01 (cyan). The dashed histogram show the two samples (p14.03.01 and p14.03.02) affected by wrong trigger run ranges (this is fixed and shown by the appropriate solid lines).

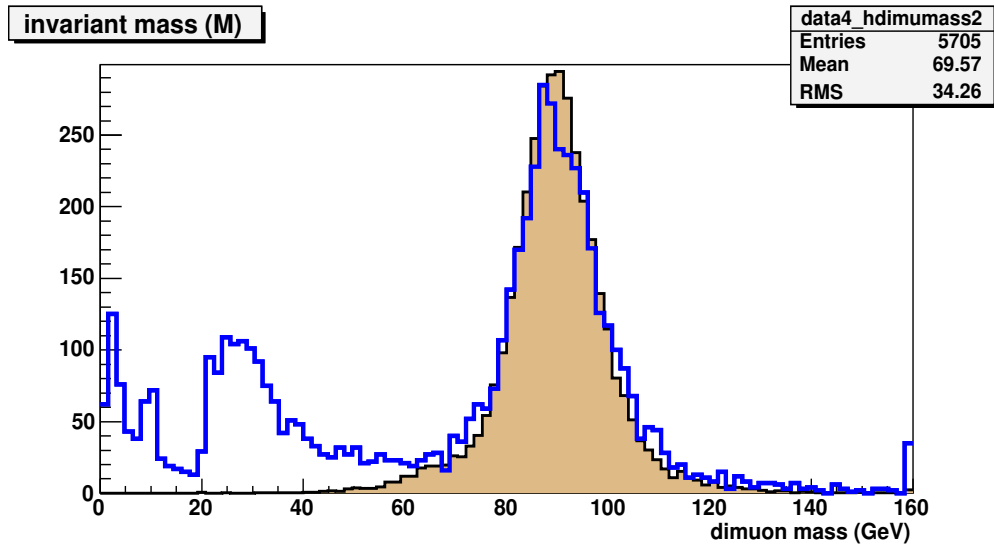


Figure 18: Distribution of the dimuon invariant mass for selected events using  $48.5 \text{ pb}^{-1}$ . The simple criteria listed in Sec. 4.3.3 have been applied.

Table 5: Measured data/MC corrections for various selection criteria. These factors are per event, not per muon.

Selection Criteria	Data/MC Correction
Calorimeter quality	$0.97 \pm 0.03$
Track $\chi^2 < 4$	$0.94 \pm 0.03$
$N_{cft} > 13$	$0.91 \pm 0.04$
Primary vertex requirement	$0.99 \pm 0.04$
Calorimeter isolation $< 2.5$ GeV	$0.99 \pm 0.04$
Track $p_T$ isolation $< 4.0(2.5)$ GeV	$0.94 \pm 0.04(0.88 \pm 0.04)$

We use the above sample to measure the data/MC corrections for several of our final selection criteria. By applying each cut one at a time (and building on each other), we measure the correction necessary to normalize the 60-120 GeV region. These tests are done using the p14.06.01 data. The measured values are presented in Table 5 while Fig. 19 shows the full data set compared to the MC normalized with these correction factors. All criteria from Table 5 are applied.

#### 4.4 $b\bar{b}$ Production

The production of a pair of  $b$  quarks is a possible source of opposite-signed dimuon events which is difficult to study due to the large cross-section. Using Pythia [10] requires full simulation of QCD events because the traditional  $b\bar{b}$  production (MSEL=5) only does the  $f\bar{f} \rightarrow b\bar{b}$  process while missing the  $f\bar{f} \rightarrow gg$  with  $g \rightarrow b\bar{b}$ . The second process becomes enhanced in this analysis since we will require the final state muons to have a fairly small opening angle ( $< 0.5$  radians).

To match the luminosity of this analysis ( $383 \text{ pb}^{-1}$ ) requires  $>200$  billion QCD events to be simulated (using a  $p_T$  cut of  $>10$  GeV on the partons). We reduce this by increasing the  $p_T$  cut at the generator level to  $> 30$  GeV. This is acceptable because the dominant contributions will be  $g \rightarrow b\bar{b} \rightarrow \mu^+\mu^-\nu\nu c\bar{c}$  and  $b \rightarrow \mu\nu c \rightarrow \mu^+\mu^-\nu\nu s$ . This still requires  $\sim 2$  billion generated QCD events. We only process events with at least two  $b$  quarks and two muons with  $p_T > 5$  GeV (d0\_mess).

We have generated a small sample ( $\sim 23\%$ ) which resulted in 60,000 events passing these criteria. These events are used to try to describe part of the dimuon spectrum (Sec. 4.5) and for a test of the background estimate (Sec. 7.3.4).

#### 4.5 Dimuon Mass Spectra

The dimuon spectrum is described at high mass completely by Z/Drell-Yan events, while at low mass numerous other sources enter. Table 6 lists the MC samples used in this analysis. Unfortunately the cross-sections for mass  $< 2$  GeV Drell-Yan,  $b\bar{b}$  and  $J/\psi$  production are too large for generation of sufficient statistics. Section 4.4 discusses a small  $b\bar{b}$  sample generated using computers at Florida State.

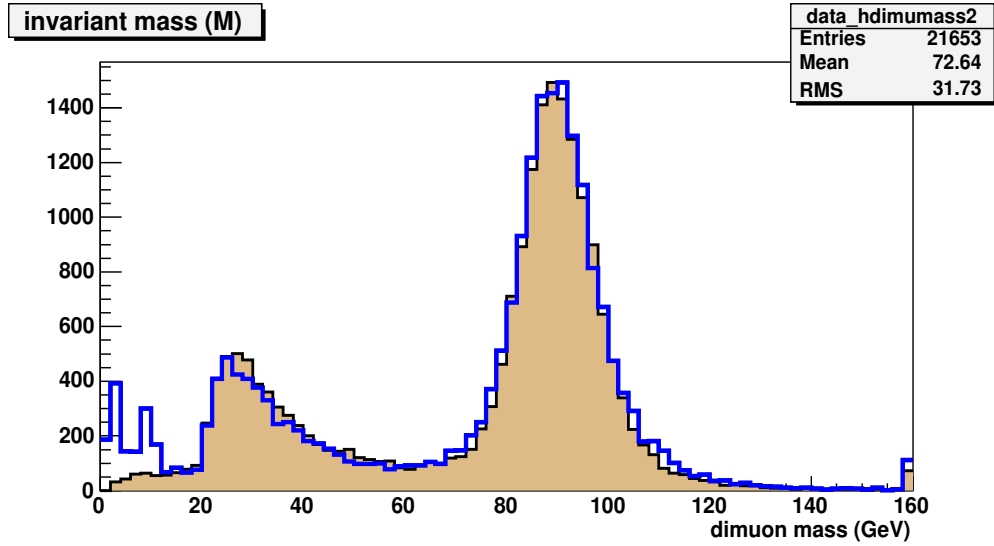


Figure 19: Distribution of the dimuon invariant mass for selected events using the full  $383 \text{ pb}^{-1}$ . The MC is normalized using the data/MC corrections listed in Table 5.

Table 6: Standard model Monte Carlo samples used in the analysis.

Process	cross-section $\times$ BR	d0_mess efficiency	K-factor	# of events	Request ids
Z/DY (m=2-15 GeV)					
( $2\mu p_T > 6 \text{ GeV}$ )	22,400 pb	0.0025	1.29	54,250	14892
Z/DY (m=15-60 GeV)	360 pb	1.0	1.35	237,000	12014, 12023, 18350
Z/DY (m=60-130 GeV)	185 pb	1.0	1.39	87,500	17231
Z/DY (m=130-250 GeV)	1.4 pb	1.0	1.39	103,250	18745
Upsilon(1S)					
( $2\mu p_T > 7 \text{ GeV}$ )	2804 pb	0.0056	1.0	34,000	11982
Upsilon(2S)					
( $2\mu p_T > 7 \text{ GeV}$ )	1402 pb	0.0082	1.0	30,000	11984
J/ $\psi$	363,000 pb	???	1.0	193,500	10932, 11684
$b\bar{b}$ (QCD $p_T > 30 \text{ GeV}$ )					
( $2\mu p_T > 5 \text{ GeV}$ )	5,140,000 pb	0.00013	1.0	40,000	N/A

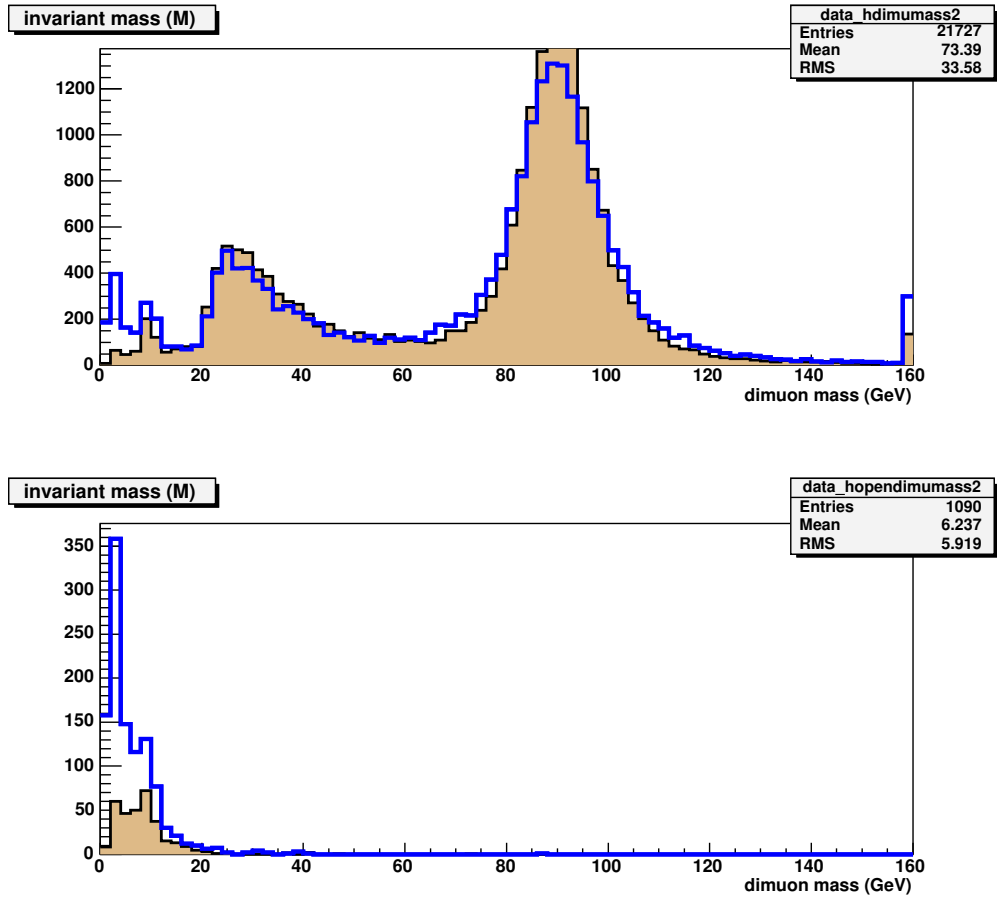


Figure 20: Distribution of the dimuon invariant mass for selected events using the full  $383 \text{ pb}^{-1}$ . The top plot uses the cuts of Sec. 4.3.2 while the bottom plot includes dimuon opening angle  $< 0.5$  radians.

We have used the high mass region to test our normalization and to measure data/MC correction factors. Figure 20 shows the spectrum out to 160 GeV before and after a cut on the opening angle is applied. Here the adjustment of the SMT/no SMT ratio has not been done. When the opening angle cut is applied, the high mass events disappear and Drell-Yan above 20 GeV becomes irrelevant.

Figure 21 zooms in on the low mass spectra which is the region of interest for this search. The blue shaded region highlights the contribution from  $b\bar{b}$  production. Several things can be noted. First, the Monte Carlo does not adequately describe the data in the  $< 10$  GeV region. Secondly, the Drell-Yan contribution is falling as you go to low mass, while the data is rising. Third, while the statistics are poor, the  $b\bar{b}$  production is nowhere near enough to account for the differences. Fourth, the  $\Upsilon(3S)$  peak is close to being described if we account for the under-estimated background and the missing  $J/\psi$  events. Fifth, the  $J/\psi$  distribution has only 2 events passing the final cuts so its statistics are too poor to say anything. How the data and MC behave under more

Table 7: Criteria for various sub-skims. The first 6 lines are applied to each muon, the remaining lines to each event.

Criteria	Subskim 1	Subskim 2	Subskim 3
$\mu$ quality	"loose"		
# of segments (muons)	nseg==3		
Central track match	Yes		
Track $\chi^2$	< 10	< 4	
$\Sigma E_{cal}(0.1 < R < 0.5)$	-	< 2.5 GeV	
# of CFT hits	> 7	> 13	
Bad runs	reject		
Calorimeter Quality	OK		
# of muons	> 1		
dimuon opening angle	-	-	< 0.5 rad
Vertex $\chi^2$	-	-	< 10
# of events	11.5M	3.3M	1.0M

stringent cuts is described in Sec. 7.1.

## 5 Data Sample

The PASS2 p14 2MU skim is used as the basis for this analysis. We include data from runs 161101 until 196579 (August 2002 - August 2004). A bad runs list is created from the run quality database [13] for runs which list the CAL, MUON, SMT or CFT system as "bad" or "special". The bad run list is extended by the *runrange\_luminosity* program used to calculate the luminosity for each trigger. In addition the program generates a bad luminosity block number (LBN) list. Events are rejected if their run or LBN is included in the respective list. Runs 172359 - 173101 are excluded due to a problem with the dimuon trigger (2MU\_A\_L2M0) with a loss of 4  $pb^{-1}$  of data. The sample results in a total integrated luminosity of  $383 \pm 25 pb^{-1}$ .

The 2MU skim was sub-skimmed from 55M (M=million) events to 11.5M events using the criteria in Table 7. A sub-subskim reduced the number to 3.3M events while a final subskim resulted in 1.012,975 data events. The muon criteria select candidates of "loose" quality [14] which have at least 3 muon segments and are matched to a central track. The central track must have a good  $\chi^2$  and a minimum number of hits in the CFT. No requirements are made on hits in the SMT. The standard calorimeter isolation cut is used, however no track  $p_T$  isolation is applied at this level (see Table 7).

At each stage we require at least 2 muons passing the muon criteria. The third subskim also limits the opening angle between the two muons as well as the  $\chi^2$  from the vertex fit. Discussion of more restrictive cuts for the final selection is included in Sec. 6.

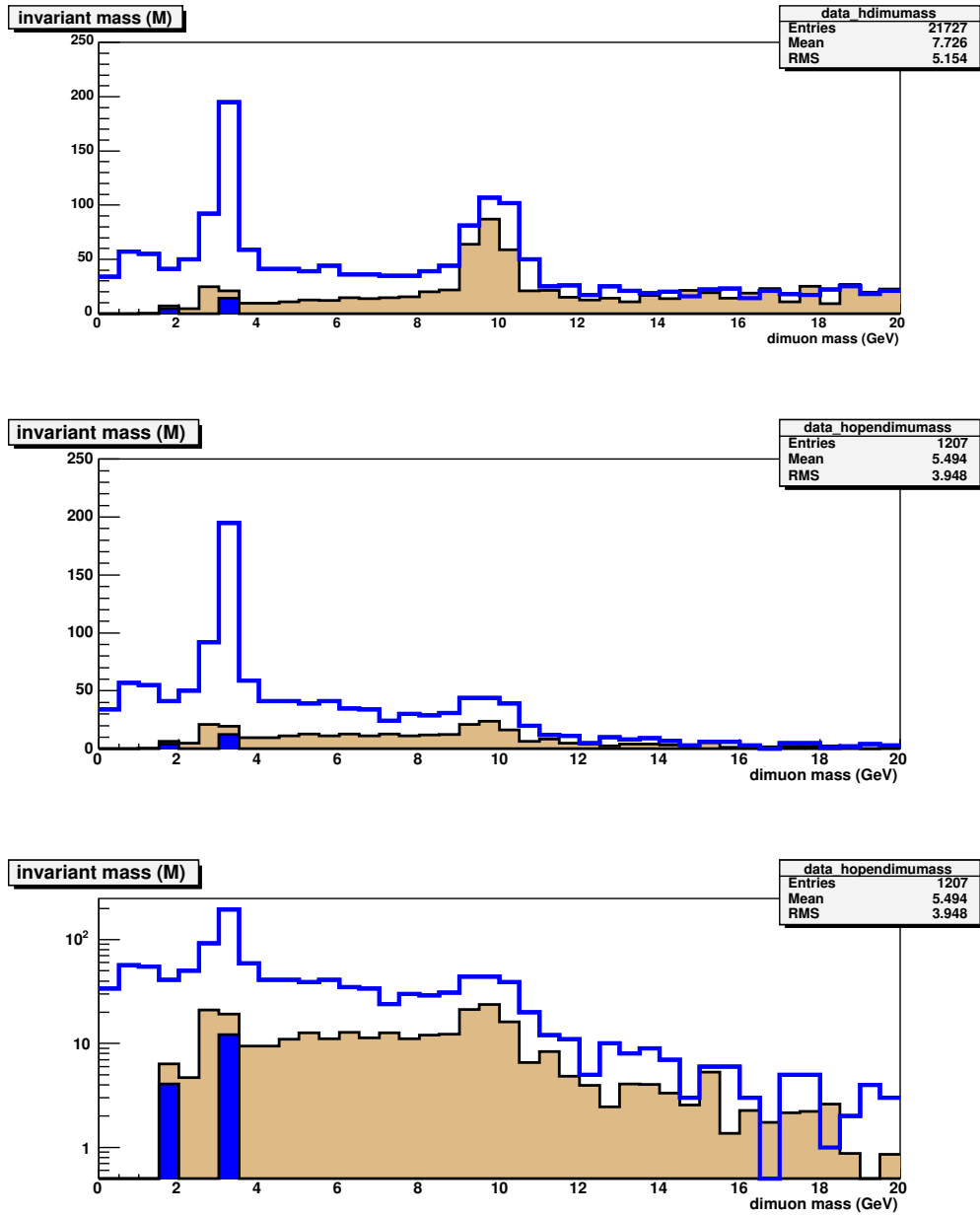


Figure 21: Distribution of the dimuon invariant mass for selected events using the full  $383 \text{ pb}^{-1}$ . The top plot uses the cuts of Sec. 4.3.2 while the bottom two plots include dimuon opening angle  $< 0.5$  radians. These two plots are identical except for the log scale on the  $y$ -axis.

Table 8: Criteria for event selection.

	Criteria	Final Sample	
muon cuts	$\mu$ quality	“loose”	sub-skim cuts
	# of segments (muons)	nseg==3	
	Central track match	Yes	
	$\Sigma E_{cal(0.1 < R < 0.5)}$	< 2.5 GeV	
	Track $\chi^2$	< 4	
	# of CFT hits	> 13	
	Cosmic ray timing cut	Yes	
	$\Sigma_{tracks} p_T(R < 0.5)$	< 2.5 GeV	
	DCA cut	Yes	
	$p_T(\mu)$	> 10 GeV	
dimuon cuts	# of muons	> 1	sub-skim cuts
	Dimuon opening angle	< 0.5 rad	
	Vertex $\chi^2$	< 4	
	Opposite-signed muons	Yes	
	Distance between muons at A-layer	> 1 cm	
	# of medium muons	> 0	
	Primary Vertex	Found	
	$ v_x $	< 0.3 cm	
	$ v_y $	< 0.3 cm	
	$ v_z $	< 60 cm	
	Dimuon trigger fired	Yes	
	Vertex radius significance	> 6	
Vertex radius	5-20 cm		

## 6 Selection Criteria

Data selection was designed to keep the signal acceptance high in order to explore the lowest possible cross-sections. However, in the low mass region ( $M < 20$  GeV) we observe a large number of dimuon events in the data that include contributions from  $J/\psi$ ,  $\Upsilon$ , Drell-Yan and  $b\bar{b}$ . These events are suppressed using the criteria discussed in the following (Table 8).

### 6.1 Event Criteria

For each event we recalculate the vertices after removing all tracks associated with muons. This avoids any bias due to the displaced vertex. We also then select the primary vertex using the *HardScatterVertex()* method from DØRoot. To ensure quality dimuon events which are well-reconstructed we require a primary vertex (PV) which is found

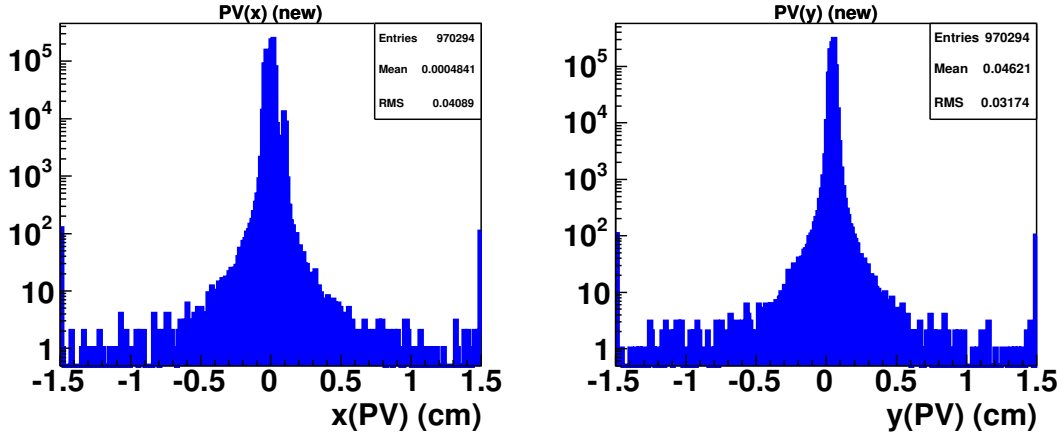


Figure 22: Distribution of the primary vertex position in  $x$  (left) and  $y$  (right).

within 0.3 cm of the beamline in  $x$  and  $y$  (Fig. 22). This reduces complications from events with increased dimuon vertex radius due to the primary vertex being mistakenly identified with large radius. A cut on the  $z$  position of the PV of within 60 cm of the detector center makes sure the interaction is well measured by the tracking system. If no primary vertex is found, the event is discarded. A dimuon trigger is required as listed in Table 9.

## 6.2 Muon Criteria

In addition to the subskim criteria listed in Sec. 5, we have added or tightened some cuts. Cosmic rays are rejected with a timing cut only. No cosmic ray distance of closest approach (DCA) rejection is applied due to the detached nature of the signal decay vertex. A cut on the distance of closest approach is discussed in Sec. 6.2.2.

Muon isolation is a bit more challenging than normal because for the signal the muons have a small opening angle. The standard calorimeter isolation ( $\sum_{0.1 < \Delta R < 0.5} E_{cal} < 2.5$  GeV) works fine (Fig. 23), however the standard track  $p_T$  cone isolation ( $\sum_{R < 0.5} p_{Ttracks}$ ) does not (Fig. 24a). A modified algorithm is described in Sec. 6.2.1.

The muon  $p_T$  ( $>10$  GeV) is selected to minimize background (Fig. 25) and ensure high trigger efficiency. As discussed in Sec. 4.3.1, we use the  $p_T$  variable for MC and data. Studies were done with  $p_T > 4$  GeV which resulted in an even larger background not described by the Monte Carlo. In addition, this sample suffered from  $> 50\%$  events failing the dimuon triggers, likely due to trigger inefficiency.

### 6.2.1 Modified Track $p_T$ Isolation Algorithm

A modified track  $p_T$  algorithm is applied to improve isolation. It sums the  $p_T$  of all tracks within a cone of  $\Delta R < 0.5$  in  $\eta - \phi$  space around the candidate muon. We exclude the track associated with the other muon in the pair if it falls within the cone. The root macro code for this algorithm is attached in Appendix A. This algorithm gives

Table 9: Dimuon triggers used in this analysis.

Trigger List	Trigger	Begin Run	End Run	Integrated Luminosity
v8-v10	2MU_A_L2M0	161101	174844	61.6 $pb^{-1}$
v11	2MU_A_L2M0_L3L15 2MU_A_L2M0_TRK10	174845	178721	61.0 $pb^{-1}$
v12	2MU_A_L2M0_L3L6 2MU_A_L2M0_TRK5	178722	194597	217.1 $pb^{-1}$
v13	DMU1_LM6 DMU1_TK5	194598	196578	48.5 $pb^{-1}$

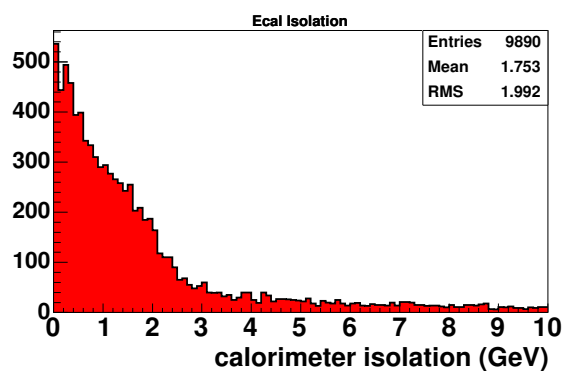


Figure 23: Distribution of the muon calorimeter isolation for the signal MC.

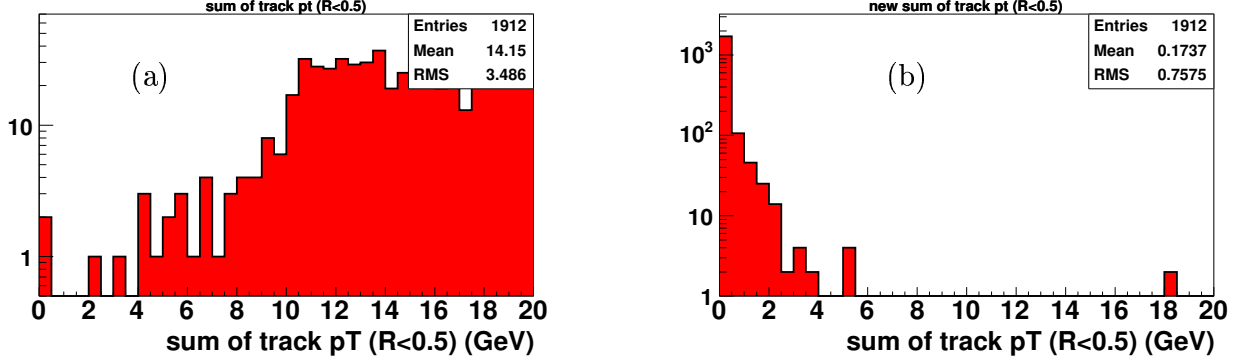


Figure 24: Distribution of the muon track isolation for signal MC. The left histogram (a) shows the standard algorithm, the modified algorithm is shown on the right.

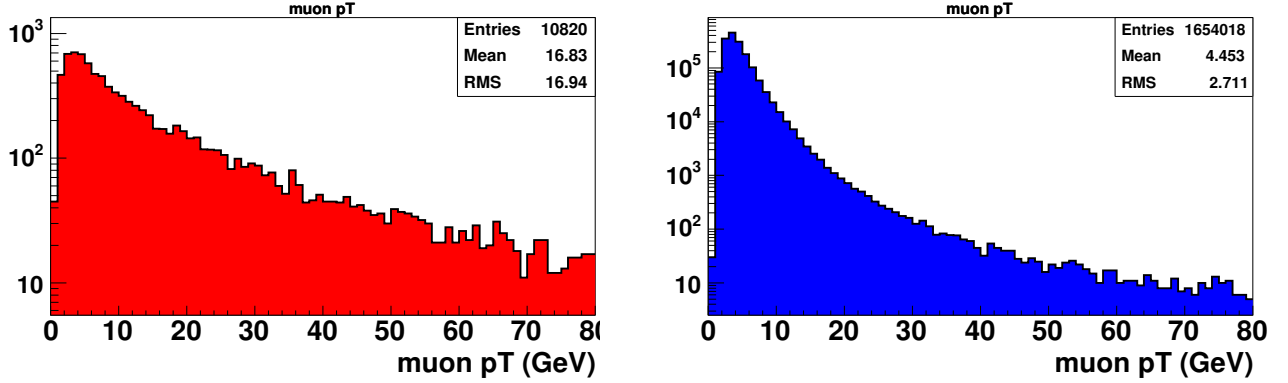


Figure 25: Distribution of muon  $p_T$  for signal (left) and data (right).

good isolation discrimination (Fig. 24b) and further rejects muons from jets with a cut at  $< 2.5$  GeV.

## 6.2.2 Distance of Closest Approach

The detached nature of the decay vertex means that muons from signal events tend to have a large distance of closest approach (DCA) to the primary vertex (Fig. 26) while most muons from standard model processes originate from the PV. The data distributions are shown in Fig. 27. We use this to reduce the physics backgrounds.

Each muon must pass the following DCA criteria for each vertex that meets the same criteria as the PV (above) and has more than 2 tracks associated with it:

1. DCA in  $x - y$  plane  $> 0.01$  cm
2. DCA in  $z$  direction  $> 0.1$  cm.

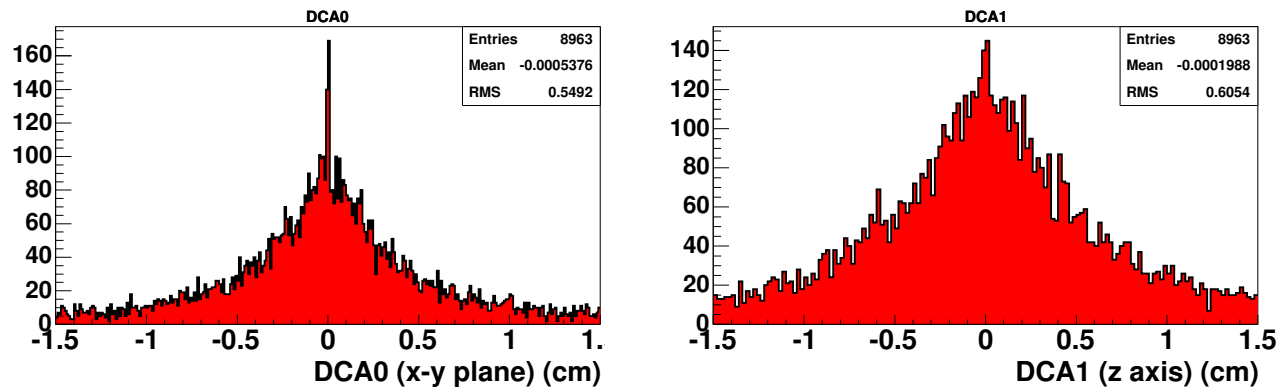


Figure 26: Distribution of distance of closest approach for signal. The left plot shows the distance in the  $x - y$  plane while the right plot is the DCA along the  $z$  axis.

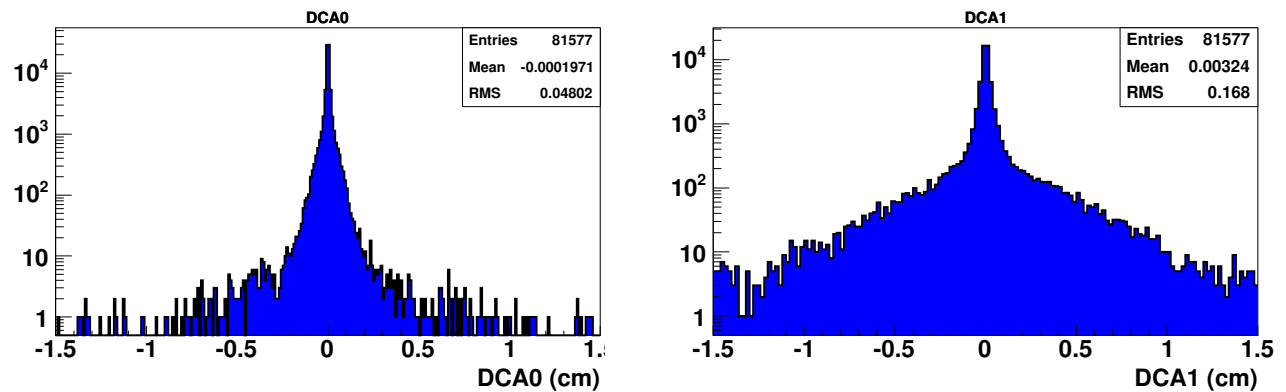


Figure 27: Distribution of distance of closest approach for data. The left plot shows the distance in the  $x - y$  plane while the right plot is the DCA along the  $z$  axis.

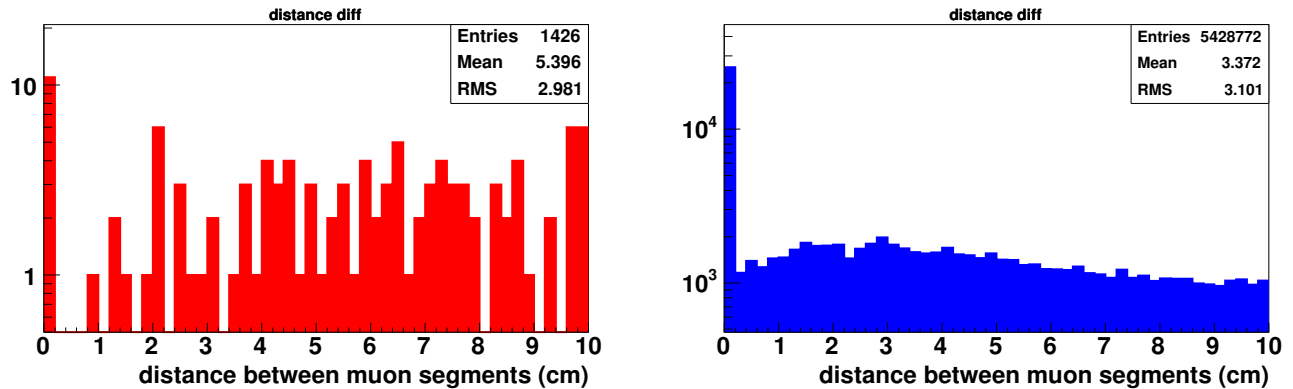


Figure 28: Distribution of distance between local muon segments at the A layer for the signal (left) and data (right). Only minimal cuts have been applied: “loose”, nseg=3, cosmic ray timing, and  $p_T > 4$  GeV.

The DCA cut will be used to define different samples of dimuon vertices (Sec. 7.2). These samples will be used to estimate our background.

### 6.3 Muon Pair Criteria

Once the muon criteria are applied, events are kept if they contain two or more muons. All combinations of muon pairs that pass the following cuts are used. A pair is rejected if both local muon segments lie within 1.0 cm of each other at the muon A layer (Fig. 28). At least one muon must be of “medium” quality. The opening angle between the muons must be less than 0.5 radians (Fig. 29). Finally, the muons must be of opposite sign, although we do look at same sign events as an indicator of backgrounds.

Each remaining pair is fit using *VertexGlobalFitter()* from DØRoot which finds the best common vertex between the two central tracks. We require that the vertex  $\chi^2 < 4$ . The dimuon mass spectrum for this sample is shown in Fig. 30. In our signal region, we also require the vertex radius to be at least  $6\sigma$  and 5 to 20 cm as measured from the primary vertex.

## 7 Estimation of the Background

### 7.1 Additional Comparisons

Figures 31 and 32 show the progression of data and SM backgrounds for several cuts. As already seen in Fig. 20 the high mass region is excluded by the opening angle cut. Table 6 shows the background samples used for the included plots.

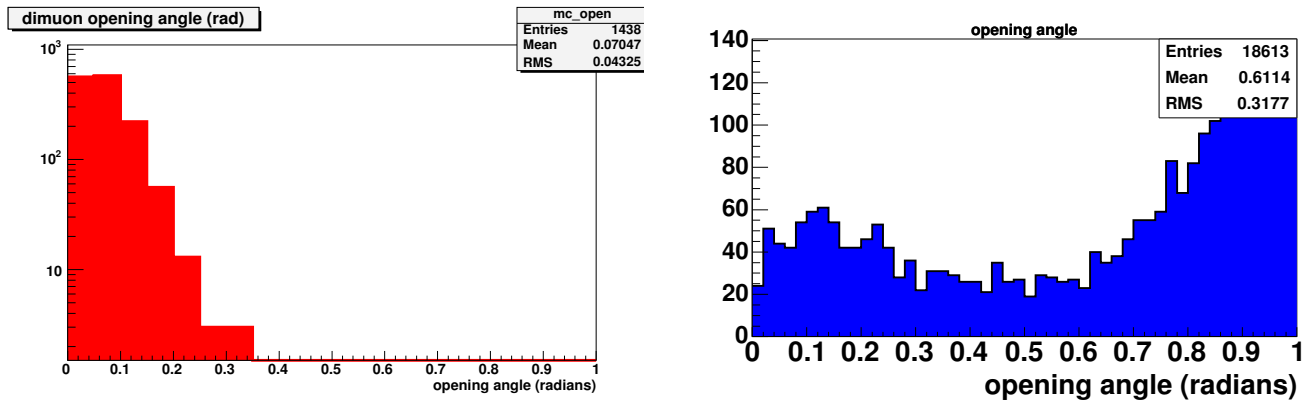


Figure 29: Distribution of dimuon opening angle for signal (left) and data (right).

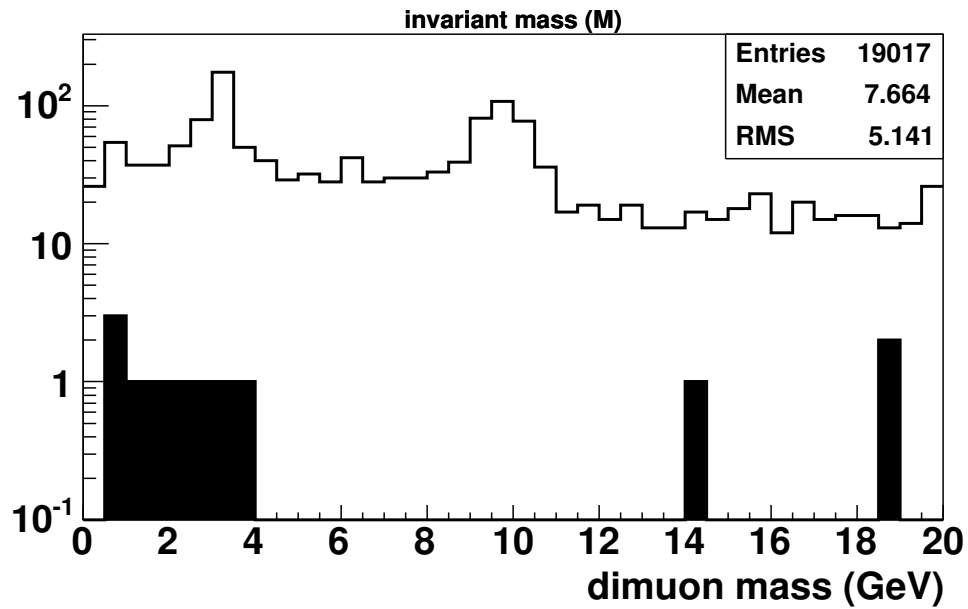


Figure 30: Distribution of the dimuon invariant mass for data. The open histogram is opposite-signed events while the filled histogram is same-signed events.

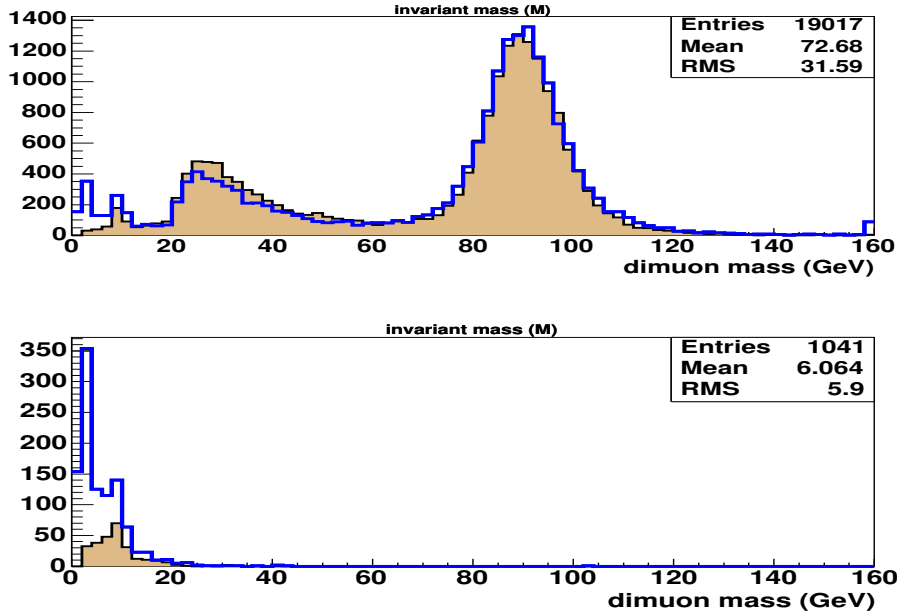


Figure 31: Distribution of the dimuon invariant mass for data (open histogram) and standard model MC (filled histogram). All cuts are applied except for the opening angle, DCA, vertex significance, and vertex radius. Background sources include  $\Upsilon$  and  $Z/DY$ . The bottom plot includes the opening angle  $< 0.5$  rad cut.

## 7.2 Background Estimate

Because of the difficulty of not being able to describe the dimuon data with MC (Fig. 21), the background within the signal region is estimated using a matrix method with the DCA and vertex radius cuts. For the DCA cut, we require either: (1) one track to pass the DCA cut and one to fail it; or (2) both tracks to pass the DCA cut. For the vertex radius we define two regions: (A)  $0.3 < \text{radius} < 5$  cm; or (B)  $5 < \text{radius} < 20$  cm. Figure 33 shows a pictorial example with the squares representing the samples 1A, 1B, 2A and 2B used in this method.

Figures 34 and 35 show the invariant mass and radius distributions for three different samples defined by the DCA cut:

**test:** both muons fail the DCA cut

**anti-box:** one muon fails and one muon passes the DCA cut

**signal:** both muons pass the DCA cut.

The test plots are shown for reference while the anti-box and signal plots show three of the four pieces of the matrix method. In each of these plots, we require the vertex radius to be at least 0.3 cm from the PV (Fig. 36). The final signal region is purposely left out. We observe 4 events in the anti-box sample with  $0.3 < r < 5$  cm and 1 event in the 5-20 cm region. There are three events in the signal plots for  $0.3 < r < 5$  cm.

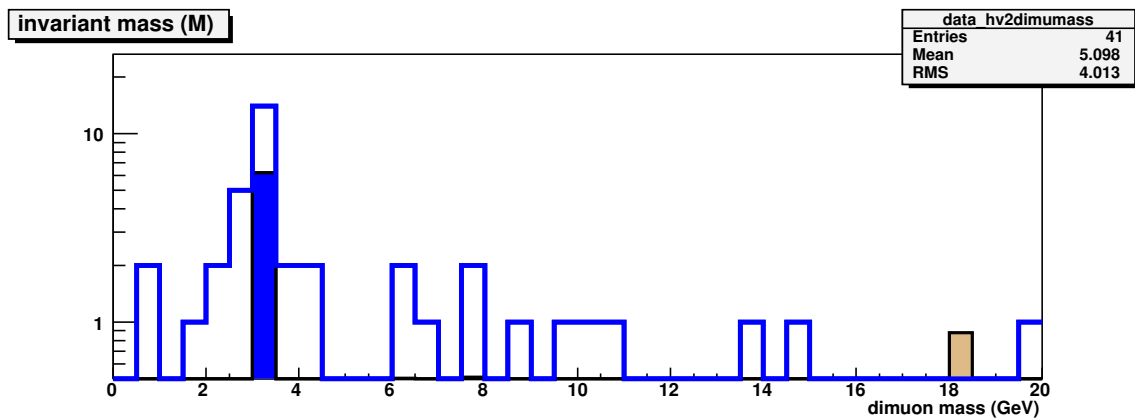
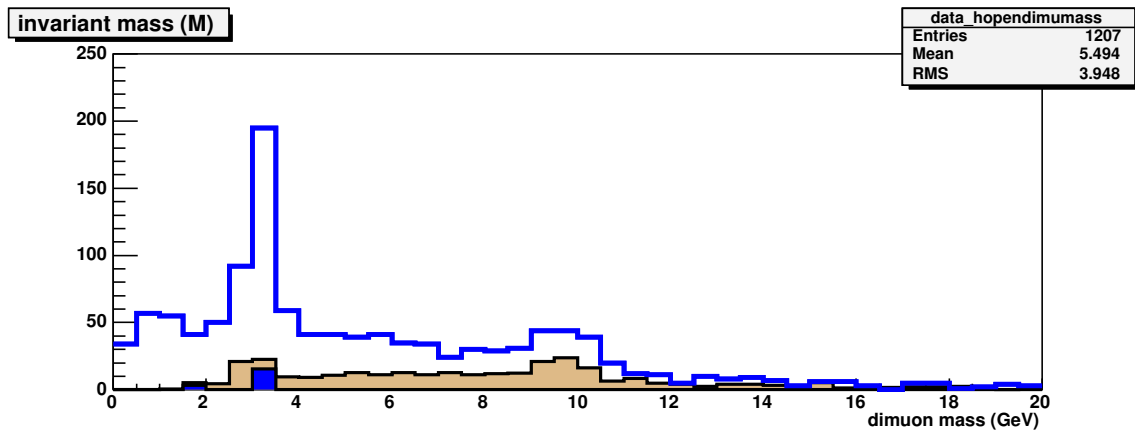
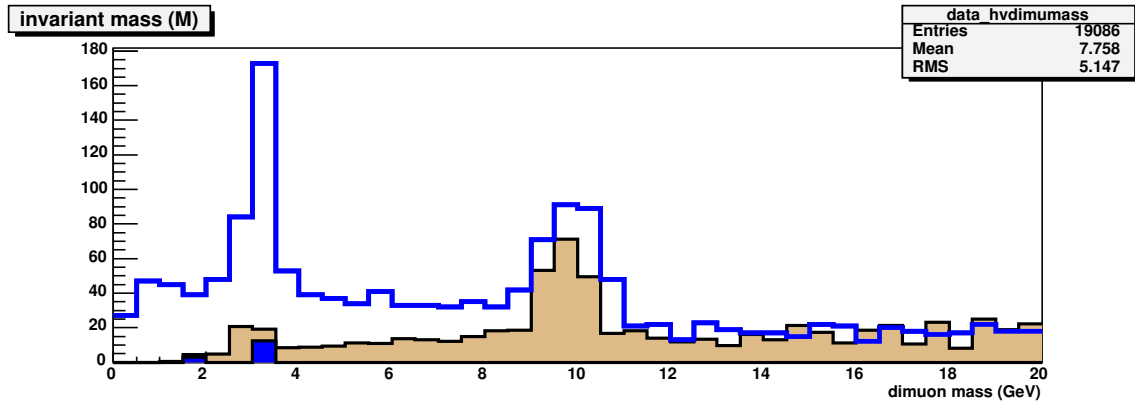


Figure 32: Distribution of the dimuon invariant mass for data (open histogram) and standard model MC (filled histogram). All cuts are applied except for the opening angle, DCA, vertex significance and the vertex reconstruction. Background sources include  $\Upsilon$  and  $Z/DY$ . The middle plot includes the opening angle  $< 0.5$  rad cut. The bottom plot includes the opening angle and vertex  $\chi^2 < 4$  cuts as well as requiring vertex radius to be less than 5 cm to exclude the signal region.

	$0.3 < r < 5 \text{ cm}$	$5 < r < 20 \text{ cm}$
one fail, one pass DCA	Sample 1A 4 events	Sample 1B 1 event
Both pass DCA	Sample 2A 3 events	Sample 2B ?? events

Figure 33: Picture of the matrix method for this analysis.

We estimate the background as:

$$background = \frac{Sample\ 2A}{Sample\ 1A} \times Sample\ 1B = \frac{3}{4} \times 1 = 0.75 \text{ events} \quad (4)$$

### 7.3 Matrix-Method Tests

There will be some correlation between DCA and vertex radius, particularly in the “fake” dimuon samples. For two particles produced at or near the PV to vertex with a large radius, one or both must be mis-reconstructed and the track will be more likely to have a large DCA. This correlation is difficult to quantify but it is likely to be limited by the fact that badly mis-reconstructed tracks won’t vertex in 3D space. Therefore, we feel the background estimate should be good to within a factor of 2 and a large error (100%) is assigned to the estimate. We describe several tests of the matrix method on complementary samples which support the assignment of this error.

#### 7.3.1 Loose Sample

One test involved loosening several cuts to expand the anti-box and signal regions to create a superset with significantly larger statistics. The following selection criteria were adjusted:

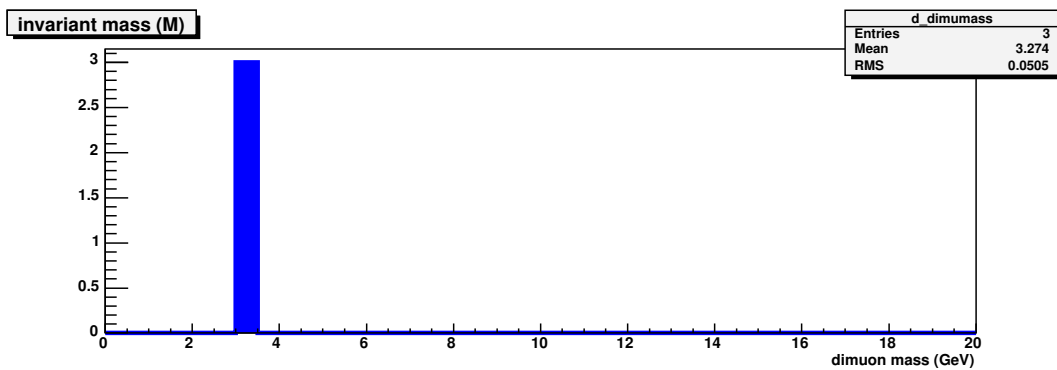
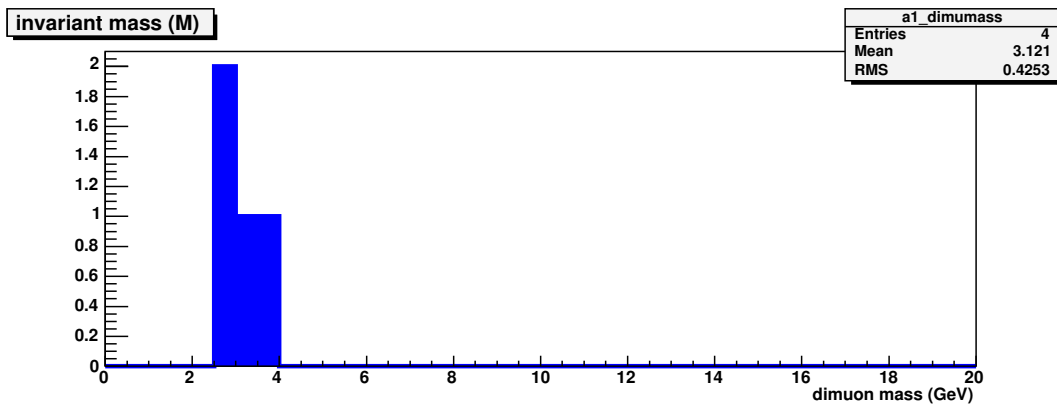
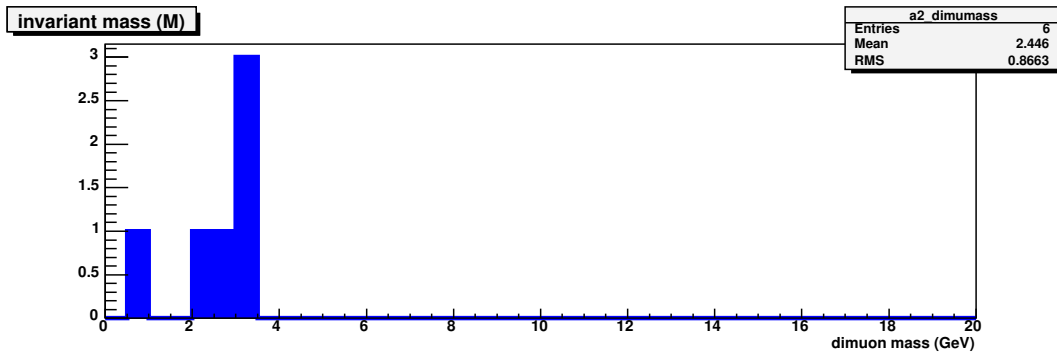


Figure 34: Distribution of dimuon invariant mass with all standard cuts except DCA and with vertex radius  $< 5$  cm. The top plot requires both muons to fail the DCA cut, the middle plot requires one muon fails and the other muon passes the DCA cut, and the bottom plot requires both muons to pass the DCA cut.

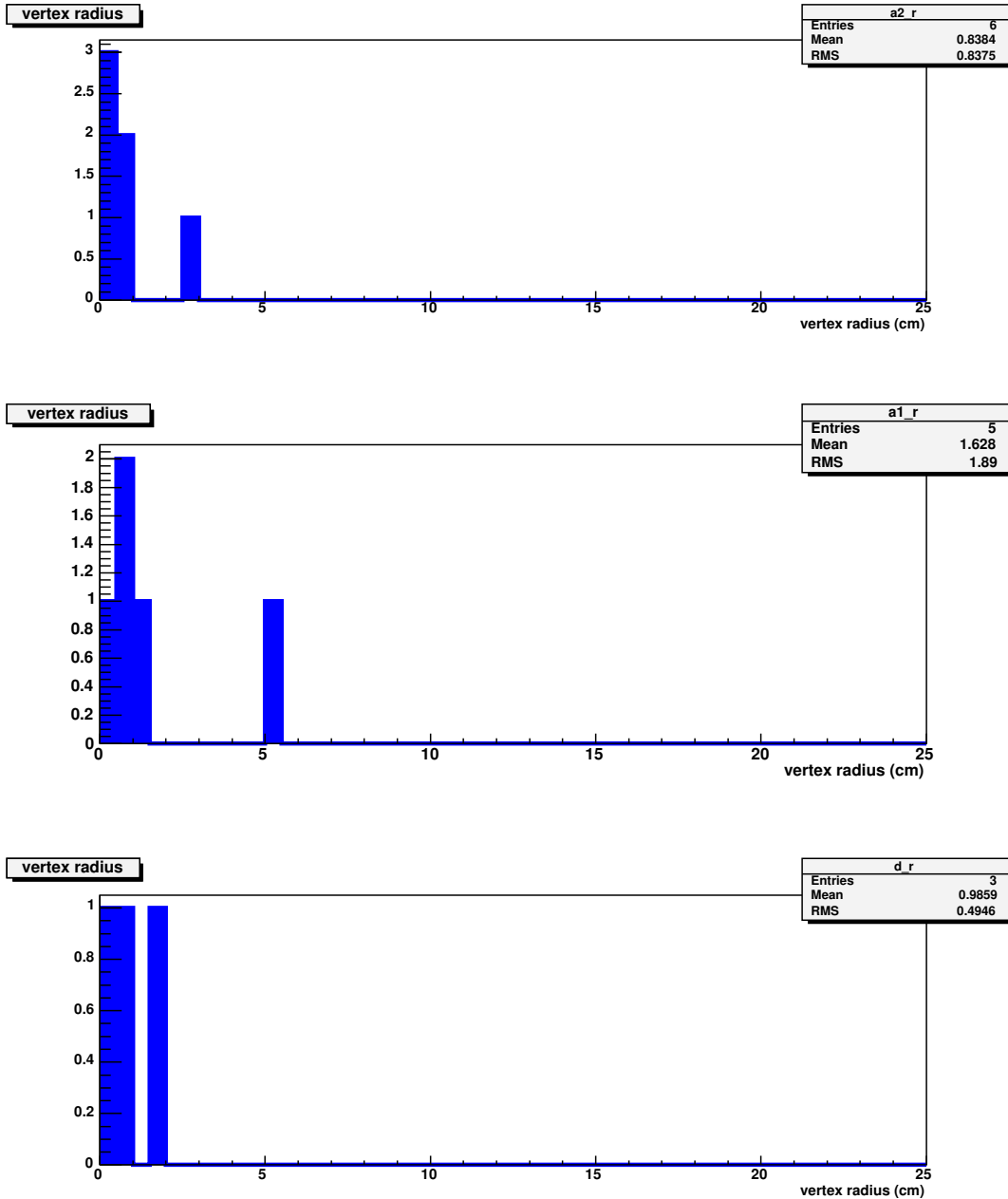


Figure 35: Distribution of vertex radius with all standard cuts except DCA. The top plot requires both muons to fail the DCA cut, the middle plot requires one muon fails and the other muon passes the DCA cut, and the bottom plot requires both muons to pass the DCA cut. For the bottom plot, an additional cut that the vertex radius  $< 5$  is applied to keep the signal region closed at this time.

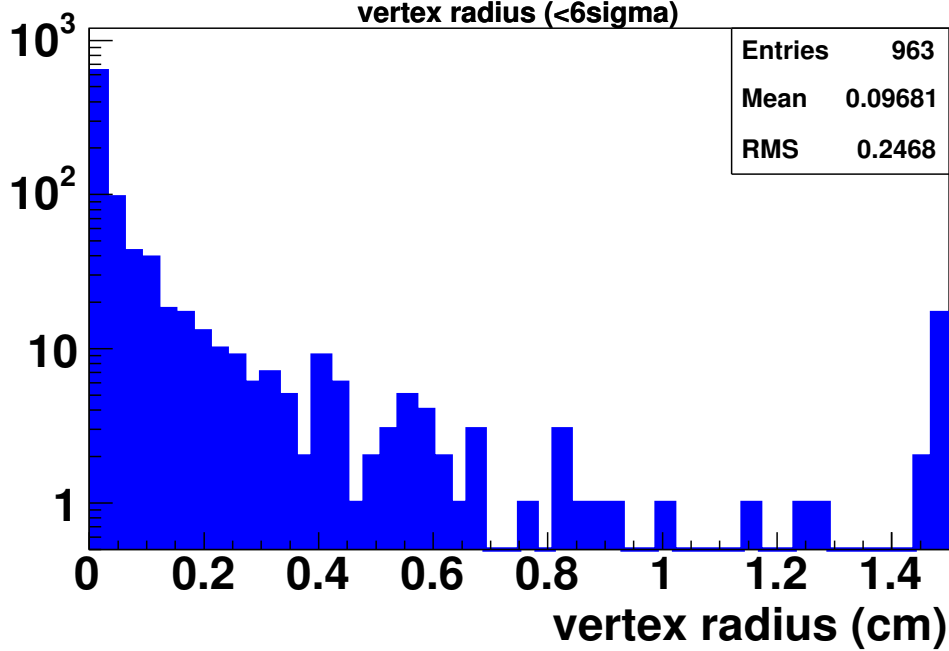


Figure 36: Distribution of the distance between the dimuon vertex and the primary vertex for vertices which are less than  $6\sigma$  away.

muon $p_T$	10 GeV	→	7 GeV
number of CFT hits	>13	→	> 10
Calorimeter isolation	<2.5 GeV	→	< 5.0 GeV
Track $p_T$ isolation	<2.5 GeV	→	removed
# of “medium” muons	>0	→	removed
vertex $\chi^2$	<4	→	< 10

This results in 383 events in Sample 1A, 152 events in Sample 2A and 25 events in Sample 1B. The matrix method predicts  $9.9 \pm 2.2$  (stat.)  $\pm 9.9$  (sys) events. We observe 21 events in Sample 2B for these cuts.

### 7.3.2 Hadron Tracks

A second test used the QCD events from the  $K_s$  analysis [7] where the invariant mass is required to be 0.6-0.9 GeV such that the  $K_s$  and baryonic sources of detached vertices are not included. In this analysis, only tracks not associated with muons are used. The loose selection criteria of the  $K_s$  analysis provide large statistics. We have performed the study using a progressively higher track  $p_T$  cut with the results summarized in Table 10. These samples are correlated, but the results are all consistent within the quoted errors.

Table 10: Results of matrix method test using two non-muon tracks above a certain  $p_T$  threshold.

$p_T$ cut	Sample				Matrix Method Estimation
	1A	2A	1B	2B	
$p_T > 2$ GeV	2216	2652	644	1578	$771 \pm 38 \pm 771$
$p_T > 4$ GeV	448	221	515	358	$254 \pm 24 \pm 254$
$p_T > 6$ GeV	148	168	98	128	$108 \pm 16 \pm 108$
$p_T > 8$ GeV	67	49	70	49	$51 \pm 11 \pm 51$
$p_T > 10$ GeV	33	39	33	26	$39 \pm 11 \pm 39$

Table 11: Results of matrix method test using one muon and one non-leptonic track.

	Sample				Matrix Method Estimation
	1A	2A	1B	2B	
no isolation no track quality	9185	2216	2257	672	$545 \pm 17 \pm 545$
no isolation track quality cuts	296	66	76	40	$16.9 \pm 3.0 \pm 16.9$
isolation no track quality	1890	434	395	103	$90.7 \pm 6.6 \pm 90.7$
isolation track quality	6	3	6	3	$3 \pm 2.4 \pm 3$

### 7.3.3 One Muon + One Pion

A third test combines a muon with a non-leptonic track. We use the dimuon subskim (subskim 1 in Table 7 and therefore require the events to pass the dimuon trigger and have 2 dimuon candidates which are "loose",  $n_{seg}=3$ , central track matched with  $p_T > 7$  GeV and at least 9 CFT hits. The dimuons must have an opening angle of at least  $\pi/2$  radians. We then pair each muon with any central tracks which lie within 0.5 radians. We reject any tracks matched within 0.05 radians of any muon or electron candidate.

The results of this study are presented in Table 11. Several combinations were done: (a) with and without calorimeter and track  $p_T$  isolation (both  $< 5.0$  GeV); (b) with and without track quality cuts on the hadronic track ( $p_T > 7$  GeV and at least 9 CFT hits).

### 7.3.4 $b\bar{b}$ Test

The  $b\bar{b}$  sample (Sec. 4.4) has been used for another matrix method test. We use the generator-level 4-vectors and apply the following cuts: muon  $p_T > 10$  GeV, muon  $|\eta| < 2.0$ , dimuon opening angle  $< 0.5$  radians. We find the point of closest approach between the two muons. Figure 37 shows the radius and distance between the tracks for this point. We calculate the DCA between the muons and the reconstructed vertex.

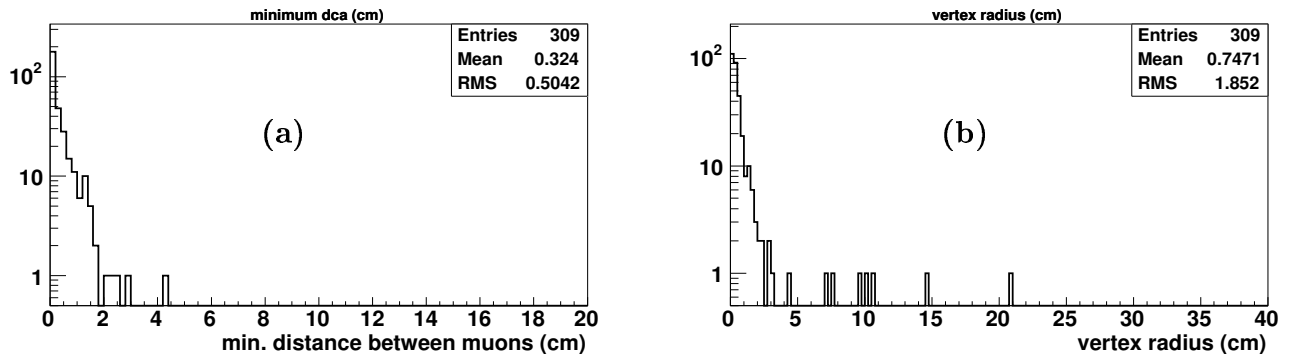


Figure 37: Distribution of the distance between the dimuon tracks at the point of closest approach (left) and the radius (distance from the beamline) for  $b\bar{b}$  generator-level 4-vectors.

A random number selects whether the track has SMT hits (0.82 probability). The DCA0 value is smeared by addition of a Gaussian with width 0.005(0.38) for tracks with(without) SMT hits. The DCA1 value is similarly smeared by a Gaussian with width 0.017(0.3). Figure 38 shows the distributions used to determine the Gaussian widths.

The DCA and vertex radius are used to test the matrix method. We find 212 events in Sample 1A, 117 events in Sample 2A, and 5 events in Sample 1B. This leads to a background estimate of  $2.8 \pm 2.1 \pm 2.8$  events. We measure 5 events in Sample 2B which is consistent with the estimation.

## 7.4 Final Background Estimate

Thus, we estimate the background in the signal region to be  $0.75 \pm 1.08$  (stat)  $\pm 0.75$  (sys) events.

## 8 OLD - Cross-section limits

For a preliminary result, we anticipate setting a limit on the pair production of NLLP. The limit is in the two dimensional space of cross-section  $\times$  BR( $\rightarrow \mu^+ \mu^-$ ) vs. lifetime. The lifetime dependence is calculated based on the fraction of events which decay within our search region and is given by:

$$\text{decay probability} = \frac{1.0 - e^{-1.0 \times \frac{L}{\tau}}}{e^{\frac{L_0}{\tau}}} \quad (5)$$

where  $L$  is the length of the decay volume (15 cm),  $L_0$  is the distance from production to the beginning of the decay volume (5 cm) and  $\ell$  is average decay length.  $\ell$  is ap-

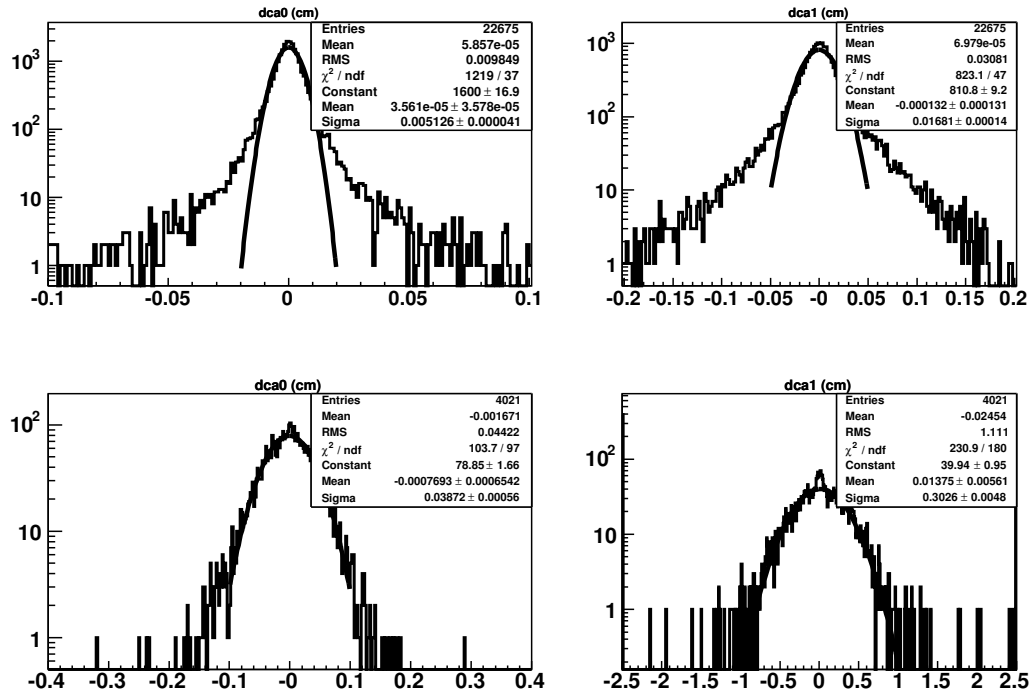


Figure 38: Distribution of DCA0(left) and DCA1(right) for dimuon data events in the mass region 60-120 GeV. The top plots are for tracks with SMT hits while the lower plots are for tracks without SMT hits. The fit is a simple Gaussian.

Table 12: Error estimation for cross-section limit. The Monte Carlo acceptance is for signal point 2 (5 GeV mass).

	Value	Error
Luminosity ( $\text{pb}^{-1}$ )	383	25
Monte Carlo acceptance	0.0547	0.0035 (stat)
Trigger acceptance <sup>1</sup>	0.90	0.10
Data/MC Calorimeter quality	0.97	0.03
Data/MC Track $\chi^2 < 4$	0.94	0.03
Data/MC $N_{cft} > 13$	0.91	0.04
Data/MC Primary vertex requirement	0.99	0.04
Data/MC Calorimeter isolation $< 2.5$ GeV	0.99	0.04
Data/MC Track $p_T$ isolation $< 2.5$ GeV	0.88	0.04
Data/MC vertex reconstruction	0.92	0.14
Luminosity $\times$ acceptance	14.2???	2.8

proximated by  $\ell = \beta\gamma c\tau$  where  $\beta = p_{Tavg}/\sqrt{p_{Tavg}^2 + m^2}$  ( $p_{Tavg}$  is the average  $p_T$  and  $m$  is the NLLP mass),  $\gamma$  is the average Lorentz boost,  $c$  is the speed of light and  $\tau$  is the lifetime.

The cross-section sensitivity depends upon the background estimate (Sec. 7.2), the number of events in the signal region (currently unknown) and the luminosity times signal acceptance. The limit further depends upon the error on these numbers. Our error estimate on the luminosity times signal acceptance is summarized in Table 12. The luminosity error is the standard 6.5% and the MC acceptance error is statistical. Tracking and muon-id data/MC corrections are estimated from another analysis, the search for RPV SUSY in the  $\mu\mu\ell$  channel [15].

We estimate the data/MC correction for vertex reconstruction from Sec. 2 using the ratio from Fig. 6 ( $1.67 \pm 0.05$ ) and the ratio of  $K_s$  candidates without vertexing ( $1.66 \pm 0.21$ ). The ratio of ratios for the candidates without vertexing to the candidates with fitting is  $(1.67 \pm 0.05)/(1.66 \pm 0.21) = 1.00 \pm 0.13$ . This is modified by the difference in tracking efficiency between data and Monte Carlo within a jet environment. Further studies within the tracking group are being undertaken, but previous results give an efficiency estimate of  $0.85 \pm 0.04$  ( $0.92 \pm 0.05$ ) for data(MC). The estimation for the ratio is taken to be  $0.92 \pm 0.05$ , accounting for correlated errors. This yields a vertex reconstruction data/MC factor of  $0.92 \pm 0.14$ .

We use the *climit* program for limit setting which is also used by the Single Top group. It uses a Bayesian technique for determining the limit [16, 17, 18]. Correlated errors can be used, however we assume the error on the background estimate is independent of the luminosity  $\times$  signal acceptance. Figure 39 shows the limit which is given for various numbers of events observed in the signal region.

We can use the various signal samples (Table 1) to explore the limit as a function of the mass (Fig. 40). The acceptance and trigger efficiencies are listed in Table 13. The analysis was tuned using the 5 GeV mass point and the acceptance falls as the mass increases due to lower efficiency to reconstruct tracks from displaced vertices and large

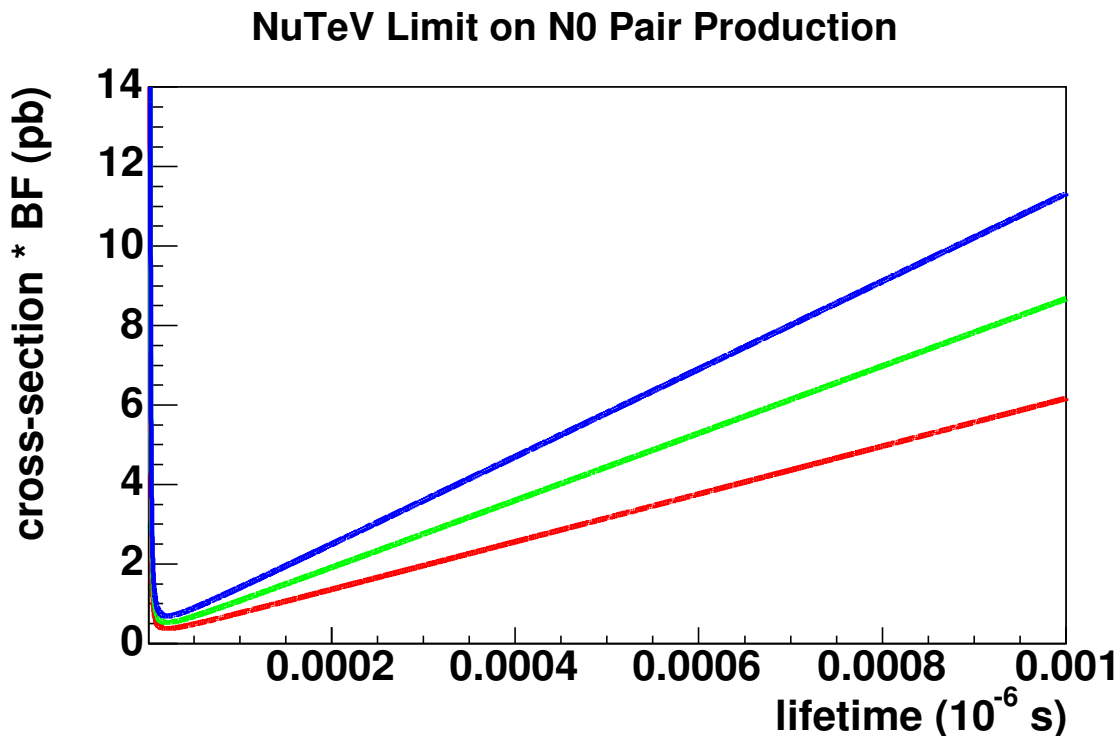


Figure 39: OLD - Limits on NLLP pair production for various number of data events observed in the signal region: 0 (red), 1 (green), 2 (blue). These apply to signal set 2 (5 GeV mass).

opening angle.

## 8.1 Comparison with NuTeV

In order to compare our results to NuTeV we must do three things: (1) convert the lifetime from NuTeV given in kilometers to seconds; (2) convert the  $pp$  cross-section at  $\sqrt{s} = 38$  GeV to a  $p\bar{p}$  cross-section at  $\sqrt{s} = 1960$  GeV; and (3) convert the NuTeV differential cross-section  $d\sigma/d\Omega$  to the cross-section  $\sigma$ . Initially, we create a copy of the NuTeV limit using Eq. 5 and empirically determining the  $y$ -axis scale factor (Fig. 41(a)). The distance to lifetime conversion (Fig. 41(b)). is done using  $\ell = \beta\gamma c\tau$  as described

Table 13: OLD - Acceptance, error and limits for the MC signal points given in Table 1. The limits are for 1 observed data event and for a lifetime of  $4 \times 10^{-11}$  s.

	Set 1	Set 2	Set 3	Set 4
$M_{\chi_0^1}$ (GeV)	3.07	5.08	8.08	10.08
acceptance	$0.0952 \pm 0.0058$	$0.114 \pm 0.0066$	$0.142 \pm 0.0075$	$0.136 \pm 0.0072$
trigger efficiency	$0.85 \pm 0.10$	$0.90 \pm 0.07$	$0.85 \pm 0.12$	$0.84 \pm 0.13$
luminosity $\times$ acceptance	$24.0 \pm 4.8$	$28.7 \pm 5.7$	$35.8 \pm 7.1$	$34.3 \pm 6.8$
limit (pb)	0.604	0.611	0.798	1.109

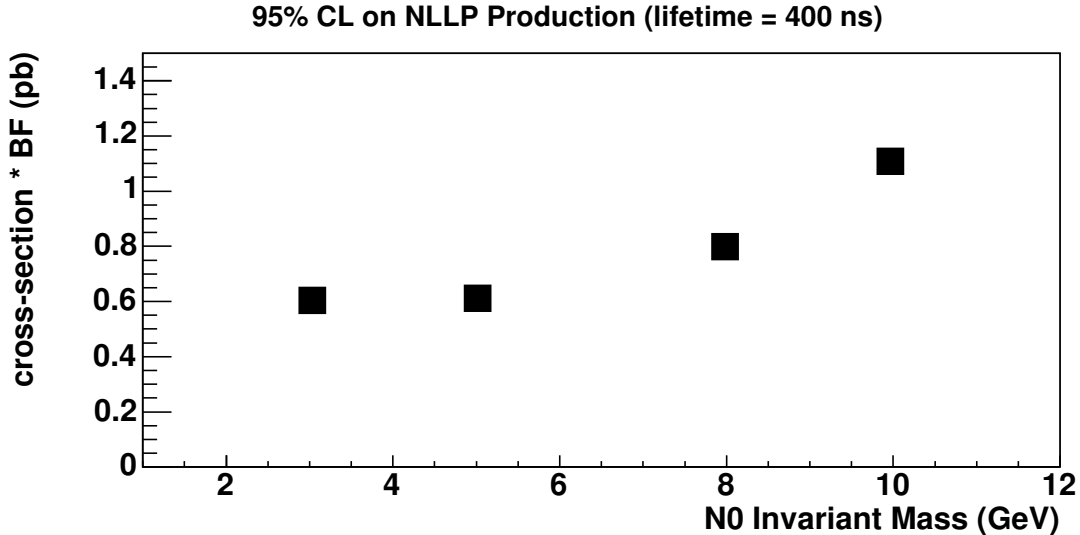


Figure 40: OLD - Limits on NLLP pair production as a function of mass. The limit is taken for 1 observed event with an NLLP lifetime of  $4 \times 10^{-11} s$ .

above.

The conversion from  $pp$  to  $p\bar{p}$  cross-section is accomplished by running SUSYGEN for both DØ and NuTeV for the 5 GeV mass point. As reported in Table 1, the  $p\bar{p}(\sqrt{s} = 1960 \text{ GeV}) = 0.0240 \text{ pb}$ . The  $pp(\sqrt{s} = 38 \text{ GeV})$  is found to be  $9.01 \times 10^{-8} \text{ pb}$ . Therefore we divide the NuTeV limit plot by  $9.01 \times 10^{-8} / 0.0240 = 266,400$ . The conversion from  $d\sigma/d\Omega$  is accomplished by multiplying the NuTeV cross-section by  $4\pi$ . Figure 42 shows a comparison of NuTeV's limit to possible limits set by DØ.

## 9 Summary

We have presented an analysis looking for neutral long-lived particles decaying to  $\mu\mu\nu$  which is a new technique that expands the capabilities of the DØ experiment. Selection criteria have been chosen to reduce the background while maintaining signal acceptance. A matrix method is used to estimate the background to be  $0.75 \pm 1.08 \pm 0.75$  events. Finally, the cross-section limits for possible observations are presented. After further review by the New Phenomena group and the Editorial Board the signal region will be explored.

## 10 Acknowledgments

We would like to thank Harrison Prosper for numerous conversations about the analysis method and for providing limit calculation programs and expertise. Don Lincoln and Ariel Schwartzman have been extremely helpful with DØRoot without which this analysis would have been virtually impossible. The DØ tracking group has provided many comments which have advanced our ability to reconstruct highly displaced vertices. Raimund Strohmer helped tremendously by determining the moun  $p_T$  smearing

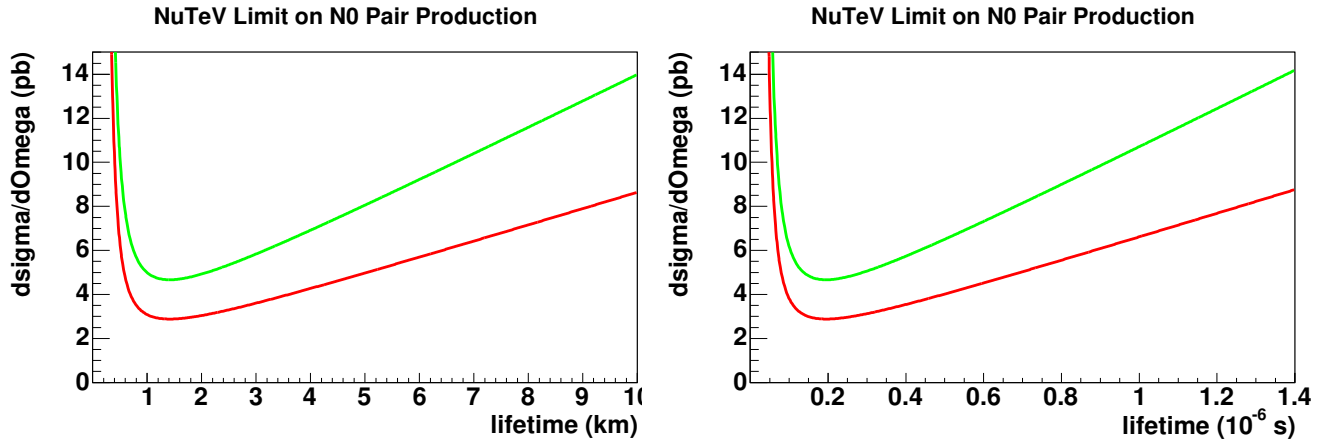


Figure 41: Reproduction of the NuTeV limit plot (left) and its conversion from distance to lifetime along the  $x$ -axis (right).

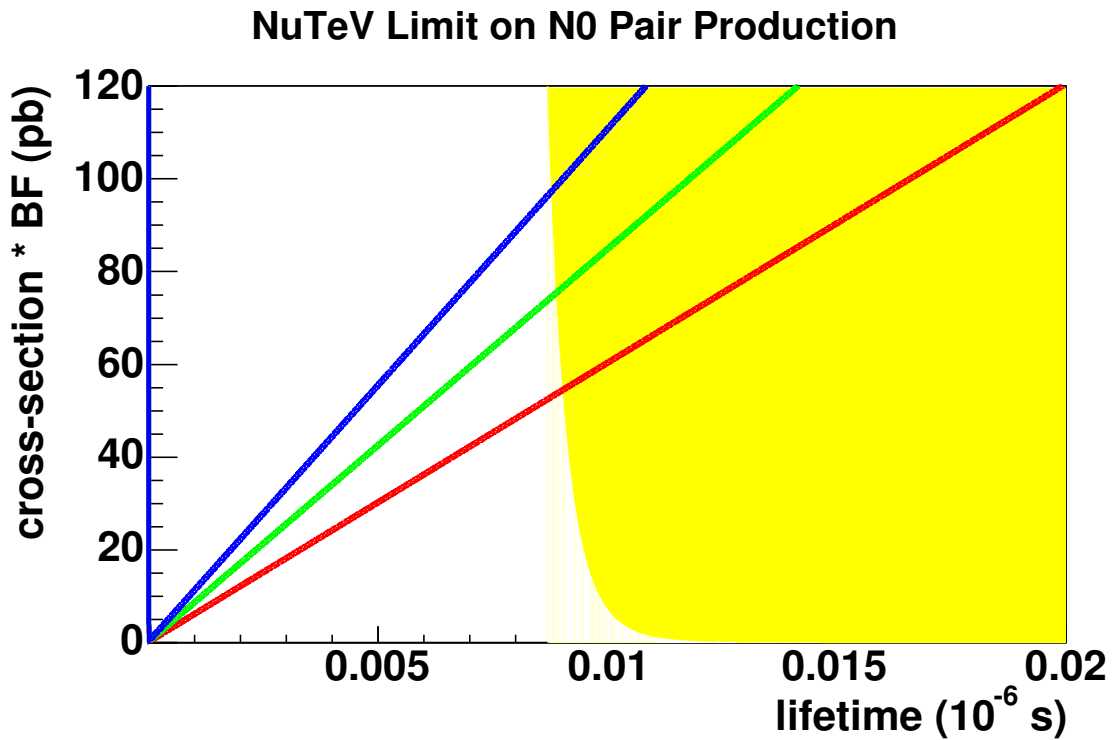


Figure 42: OLD - Comparison of  $D\bar{O}$  and NuTeV cross-section limits. This is only for general comparison at this point (it is not accurate). The curves on the right represent NuTeV while the curves on the left are for  $D\bar{O}$ .

parameters used in this analysis.

## A Appendix A - New $p_T$ Isolation Algorithm for NLLP Search

```

////////////////////////////////////
// Modified track pt isolation algorithm which doesn't include the
// other track in a pair of tracks.
// Inputs:
//   m1: muon used as center of pt cone
//   trk2: second track to be excluded from the sum
//   tlist: list of all tracks to be considered in the sum
// Output:
//   ptsum: sum of all tracks in the cone (excluding muons)
//   newTrkPtIsolation: number of tracks used in the sum
//
int newAlgorithms::newTrkPtIsolation(D0Muon *m1, D0Track *trk2, TObjArray
tlist, float *ptsum) {  int nclosetrk = 0, nreject = 0;
    float closetrkpT = 0.0;
    D0Track *t1 = (D0Track *)m1->GetTrack();
    TVector3 tv1(t1->Px(),t1->Py(),t1->Pz());
    // Loop over all tracks
    for (int ij=0; ij<tlist.GetEntries();ij++) {
        D0Track *t2 = (D0Track *)tlist[ij];
        if (t2->Pt()>0.0) {
            TVector3 tv2(t2->Px(),t2->Py(),t2->Pz());
            float tmpdeltar = tv1.DeltaR(tv2);
            if (t1!=trk2) {
                if (t2==trk2) {
                    // don't include in sum
                } else {
                    if ((tmpdeltar>0.0)&&(tmpdeltar<0.5)) {
                        nclosetrk++;
                        closetrkpT += t2->Pt();
                    }
                }
            }
        }
    }
    *ptsum = closetrkpT;
    return nclosetrk;
}

```

## References

- [1] T. Adams *et al.* [NuTeV Collaboration], “Observation of an anomalous number of dimuon events in a high energy neutrino beam,” *Phys. Rev. Lett.* **87**, 041801 (2001) [arXiv:hep-ex/0104037].
- [2] J. A. Formaggio *et al.* [NuTeV Collaboration], “Search for a 33.9-MeV/ $c^2$  neutral particle in pion decay,” *Phys. Rev. Lett.* **84**, 4043 (2000) [arXiv:hep-ex/9912062].
- [3] A. Vaitaitis *et al.* [NuTeV Collaboration], “Search for neutral heavy leptons in a high-energy neutrino beam,” *Phys. Rev. Lett.* **83**, 4943 (1999) [arXiv:hep-ex/9908011].
- [4] B. Armbruster *et al.* [KARMEN Collaboration], “Anomaly in the time distribution of neutrinos from a pulsed beam stop source,” *Phys. Lett. B* **348**, 19 (1995).
- [5] L. Borissov, J. M. Conrad and M. Shaevitz, “Searching for the lightest neutralino at fixed target experiments,” arXiv:hep-ph/0007195.
- [6] V. M. Abazov *et al.* [D0 Collaboration], “A search for the flavor-changing neutral current decay  $B_s^0 \rightarrow \mu^+ \mu^-$  in p anti-p collisions at  $\sqrt{s} = 1.96$ -TeV with the DØ detector,” *Phys. Rev. Lett.* **94**, 071802 (2005) [arXiv:hep-ex/0410039].
- [7] T. Adams, “A Study of Highly Displaced, Detached Vertices with  $K_s$ ’s Using DØRoot,” DØ Note 4671.
- [8] S. P. Martin, “A supersymmetry primer,” in Kane, G.L. (ed.): *Perspectives on supersymmetry*, p. 1-98. arXiv:hep-ph/9709356.
- [9] N. Ghodbane, S. Katsanevas, P. Morawitz, E. Perez, *SUSYGEN 3*, hep-ph/9909499.
- [10] T. Sjstrand, P. Edn, C. Friberg, L. Lnnblad, G. Miu, S. Mrenna and E. Norrbin, *Computer Phys. Commun.* **135** (2001) 238 (LU TP 00-30, hep-ph/0010017).
- [11] B. Tiller and T. Nunnemann, “Measurement of the Differential  $Z^0$ -boson Production Cross-section as Function of Transverse Momentum,” DØ Note 4660.
- [12] M. Agelou *et al.*, “Tog Trigger Efficiency Measurements at the top\_trigger package,” DØ Note 4512.
- [13] DØ Offline Run Quality Database, <http://d0db.fnal.gov/qualitygrabber/qualQueries.html>
- [14] C. Clement *et al.*, “MuonID Certification for p14,” DØ Note 4350.
- [15] D. Kafer and A. Meyer, “A Search for RPV SUSY via the  $LL\bar{E}$  Coupling  $\lambda_{122}$  in the  $\mu\mu\ell$  ( $\ell = e, \mu$ ) Channel,” DØ Note NNNN (in preparation), available from the New Phenomena web page “Analyses under review.”
- [16] I. Bertram *et al.*, “A Recipe for the Construction of Confidence Limits,” DØ Note 3476.
- [17] P. Bhat, H. Prosper and S. Synder, “Bayesian Analysis of Multi-Source Data,” *Phys. Lett. B* **407**, 73 (1997).
- [18] V. Buescher *et al.*, “Recommendation of the Ad-Hoc Committee on Limit-Setting Procedures to be Used by DØ in Run II,” DØ Note 4629.